# Evaluation of lipid biomarkers as proxies for sea ice and ocean temperatures along the Antarctic continental margin

Nele Lamping[1], Juliane Müller[1,2,3], Jens Hefter[1], Gesine Mollenhauer[1,2,3], Christian Haas[1], Xiaoxu Shi[1], Maria-Elena Vorrath[1], Gerrit Lohmann[1,3,4], Claus-Dieter Hillenbrand[5]

[1]Alfred Wegener Institute, Helmholtz Center for Polar and Marine Research, Am Alten Hafen 26, 27568 Bremerhaven, Germany

[2]Department of Geosciences, University of Bremen, Klagenfurter Straße, 28359 Bremen, Germany

[3]Marum - Center for Marine Environmental Sciences, Leobener Straße 8, 28359 Bremen, Germany

[4]Department of Environmental Physics, University of Bremen, 28359 Bremen, Germany

[5]British Antarctic Survey, High Cross, Madingley Road, Cambridge CB3 0ET, United Kingdom

*Correspondence to: Nele Lamping (nele.lamping@awi.de)*

**Abstract**

The importance of Antarctic sea ice and Southern Ocean warming has come into the focus of polar research during the last couple of decades. Especially around West Antarctica, where warm water masses approach the continent and where sea ice has declined, the distribution and evolution of sea ice play a critical role for the stability of nearby ice shelves. Organic geochemical analyses of marine seafloor surface sediments from the Antarctic continental margin allow an evaluation of the applicability of biomarker-based sea ice and ocean temperature reconstructions in these climatically sensitive areas. We analysed highly branched isoprenoids (HBIs), such as the sea-ice proxy $IPSO_{25}$ and phytoplankton-derived HBI-trienes, but also phytosterols and isoprenoidal glycerol dialkyl glycerol tetraethers (GDGTs), which are established tools for the assessment of primary productivity and ocean temperatures, respectively. The combination of $IPSO_{25}$ with a phytoplankton marker (*i.e.* the $PIPSO_{25}$ index) permits semi-quantitative sea-ice reconstructions and avoids misleading over- or

underestimations of sea-ice cover. Comparisons of the $PIPSO_{25}$-based sea-ice distribution patterns and $TEX^{L}_{86}$- and RI-OH'-derived ocean temperatures with (1) sea-ice concentrations obtained from satellite observations and (2) instrument measurements of sea surface and subsurface temperatures corroborate the general capability of these proxies to determine oceanic key variables properly. This is further supported by model data. We also highlight specific aspects and limitations that need to be taken into account for the interpretation of such biomarker data and discuss the potential of $IPSO_{25}$ as an indicator for the former occurrence of platelet ice and/or the export of ice shelf water.

## 1. Introduction

One of the key components of the global climate system, influencing major atmospheric and oceanic processes, is floating on the ocean's surface at high latitudes – sea ice (Thomas, 2017). Southern Ocean sea ice is one of the most strongly changing features of the Earth's surface as it experiences considerable seasonal variabilities with sea-ice extent decreasing from a maximum of 20 x $10^6$ $km^2$ in September to a minimum of 4 x $10^6$ $km^2$ in March (Arrigo et al., 1997; Zwally, 1983). This seasonal waxing and waning of sea ice substantially modifies deep-water formation, influences the ocean-atmosphere exchange of heat and gas and strongly affects surface albedo and radiation budgets (Abernathey et al., 2016; Nicholls et al., 2009; Turner et al., 2017). Moreover, sea ice regulates ocean buoyancy flux, upwelling and primary production (Schofield et al., 2018).

Based on the 40-year satellite record, Southern Ocean sea-ice extent as a whole followed an increasing trend (Comiso et al., 2017; Parkinson and Cavalieri, 2012), experiencing an abrupt reversal from ca. 2015 to 2018 (Parkinson, 2019; Turner et al., 2020; Wang et al., 2019), which has been attributed to a decades-long oceanic warming and increased advection of atmospheric heat (Eayrs et al., 2021). However, the sea-ice extent around major parts of West Antarctica has been decreasing over the last 40 years (Parkinson and Cavalieri, 2012). The Antarctic Peninsula is particularly affected by a significant reduction in sea-ice extent and rapid atmospheric and oceanic warming (Etourneau et al., 2019; Li et al., 2014; Massom et al., 2018; Vaughan et al., 2003). The Larsen A and B ice shelves on the east coast of the Antarctic Peninsula collapsed in 1995 and 2002, respectively. These collapses were triggered by the loss of a sea-ice buffer, which enabled an increased flexure of the ice-shelf margins by ocean swell (Massom et al., 2018). Along the Pacific margin of West Antarctica, the Bellingshausen and Amundsen seas have also been affected by major sea-ice decline and regional surface ocean warming (Hobbs et al., 2016; Parkinson, 2019). Marine-terminating glaciers draining into the Amundsen and Bellingshausen seas are thinning at an alarming rate, which has been linked to sub-ice shelf melting caused by relatively warm Circumpolar Deep Water (CDW) incursions into sub-ice shelf cavities (*e.g.*, Jacobs et al., 2011; Khazendar et al., 2016; Nakayama et al., 2018; Rignot et al., 2019; Smith et al., 2017). The disintegration of ice shelves reduces the buttressing effect that they exert on ice grounded further upstream, which can lead to partial or total loss of the ice in the catchments of the affected

glaciers and, thus, raise global sea level considerably (3.4 to 4.4 m in case of a total West Antarctic Ice Sheet collapse; Fretwell et al., 2013; Jenkins et al., 2018; Pritchard et al., 2012; Vaughan, 2008). State-of-the-art climate models are not yet fully able to depict sea-ice seasonality and sea-ice cover, which the 5$^{th}$ Assessment Report of the Intergovernmental Panel on Climate Change (Stocker et al., 2013) attributes to a lack of validation efforts using proxy-based sea-ice reconstructions. Knowledge about (paleo-)sea-ice conditions and ocean temperatures in the climate sensitive areas around the West Antarctic Ice Sheet is hence considered as crucial for understanding past and future climate evolution.

To date, the most common proxy-based sea-ice reconstructions in the Southern Ocean utilize fossil assemblages of sympagic (*i.e.* living within sea ice) diatoms preserved within the seafloor sediments (Allen et al., 2011; Armand and Leventer, 2003; Crosta et al., 1998; Esper and Gersonde, 2014; Gersonde and Zielinski, 2000; Leventer, 1998). Dissolution effects within the water column or after deposition, however, determine the preservation of small, lightly silicified diatom taxa and therefore can alter the assemblage record, leading to inaccurate sea-ice reconstructions (Leventer, 1998; Zielinski et al., 1998). Recently, the molecular remains of certain diatom taxa, i.e. specific organic geochemical lipids, have emerged as a potential proxy for reconstructing past Antarctic sea-ice cover (Barbara et al., 2013; Collins et al., 2013; Crosta et al., 2021; Denis et al., 2010; Etourneau et al., 2013; Lamping et al., 2020; Massé et al., 2011; Vorrath et al., 2019; 2020). Specifically, a di-unsaturated highly branched isoprenoid (HBI) alkene (HBI diene, $C_{25:2}$) has been detected in both sea-ice diatoms from the Southern Ocean and Antarctic marine sediments (Johns et al., 1999; Massé et al., 2011; Nichols et al., 1988). Recently, the sympagic diatom *Berkeleya adeliensis*, which preferably proliferates in platelet ice, has been identified as the producer of these HBI alkene (Belt et al., 2016; Riaux-Gobin and Poulin, 2004). However, *B. adeliensis* seems rather flexible concerning its habitat, since it was also recorded in the bottom ice layer and is apparently well adapted to changes in texture during ice melt (Riaux-Gobin et al., 2013). Belt et al. (2016) introduced the term $IPSO_{25}$ ("Ice Proxy of the Southern Ocean with 25 carbon atoms") by analogy to the counterpart $IP_{25}$ in the Arctic. Commonly, for a more detailed assessment of sea-ice conditions, $IP_{25}$ in the Arctic Ocean and $IPSO_{25}$ in the Southern Ocean have been measured alongside complementary phytoplankton-derived lipids, such as sterols and/or HBI-trienes, which are indicative of open-water conditions (Belt and Müller, 2013; Lamping et al., 2020; Etourneau

et al., 2013; Vorrath et al., 2019; 2020). The combination of the sea-ice biomarker and a phytoplankton biomarker, the so-called $PIPSO_{25}$ index (Vorrath et al., 2019), allows for a more quantitative differentiation of contrasting sea-ice settings and helps to avoid misinterpretations of the absence of $IPSO_{25}$. An absence of the sea-ice biomarker can result from either a lack of sea-ice cover or a permanent thick sea-ice cover that prevents light penetration and hence limits ice algae growth. These two contrasting scenarios can be distinguished by using the additional phytoplankton biomarker. Recently, Lamping et al. (2020) used the $PIPSO_{25}$ index to reconstruct changes in sea-ice conditions during the last deglaciation of the Amundsen Sea shelf, which were likely linked to advance and retreat phases of the Getz Ice Shelf.

Multiple mechanisms exist that can cause ice-shelf instability. As previously mentioned, relatively warm CDW is considered one of the main drivers for ice-shelf thinning in the Amundsen Sea and Bellingshausen Sea sectors of the West Antarctic Ice Sheet (Nakayama et al., 2018; Jenkins and Jacobs, 2008; Rignot et al., 2019). Accordingly, changing ocean temperatures are another crucial factor for the stability of the marine-based ice streams draining most of the West Antarctic Ice Sheet (e.g., Colleoni et al., 2018). As for sea-ice reconstructions, organic geochemical lipid proxies have been employed over the past decades for reconstructing ocean temperatures in high latitudes, since the abundance and preservation of calcareous microfossils commonly used for such reconstructions is very poor in polar marine sediments (e.g., Zamelczyk et al., 2012). In contrast, archaeal isoprenoidal glycerol dialkyl glycerol tetraethers (isoGDGTs), sensitive to temperature change and relatively resistant to degradation processes, are well preserved in all types of marine sediments (Huguet et al., 2008; Schouten et al., 2013). Schouten et al. (2002) found that the number of rings in sedimentary GDGTs is correlated with surface water temperatures and developed the first archaeal lipid paleothermometer $TEX_{86}$, a ratio of certain GDGTs, as a sea surface temperature (SST) proxy. For polar oceans, Kim et al. (2010) developed a more specific calibration model for temperatures below 15 °C, $TEX^{L}_{86,}$ which employs a different GDGT combination. There is an emerging consensus that GDGTs predominantly reflect subsurface ocean temperatures (SOT) along the Antarctic margin (Kim et al., 2012; Etourneau et al., 2019; Liu et al., 2020). This is supported by observations of elevated archaeal abundances (and GDGTs) in warmer

subsurface waters (Liu et al., 2020; Spencer-Jones et al., 2021). Archaea adapt their membrane in cold waters by adding hydroxyl groups and changing the number of rings, OH-GDGTs (Fietz et al., 2020). Huguet et al. (2017) found in molecular dynamic simulations that the additional hydroxyl moieties lead to an increase of the membrane fluidity, which aids trans-membrane transport in cold environments. This explains the higher relative abundance of OH Archaea lipids in cold environments. Taking the OH-GDGTs into account, Lü et al. (2015) proposed an SST-proxy for the polar oceans, the RI-OH'.

The aim of our study is to provide insight into the application of biomarkers in Southern Ocean sediments as sea ice and ocean temperature proxies. Estimates on recent sea-ice coverage and ocean temperatures along the eastern and western Antarctic Peninsula (EAP and WAP) as well as in the Amundsen and Weddell seas are based on the analyses of $IPSO_{25}$, HBI-trienes and phytosterols and GDGTs in seafloor surface sediment samples from these areas. A comparison of biomarker-derived estimates of sea-ice extent and ocean temperature with (1) sea-ice distributions obtained from satellite observations and (2) in-situ ocean temperature measurements allows for an evaluation of the proxy approach. We further consider AWI-ESM2 climate model data to assess the model's performance in depicting recent oceanic key variables and to examine the potential impact of paleoclimate conditions on the biomarker composition of the investigated surface sediments. Taking into account the various factors affecting the use of marine biomarkers as paleoenvironmental proxies, we comment on the limitations of GDGT temperature estimates and the novel $PIPSO_{25}$ approach. Furthermore, we discuss the potential connection between $IPSO_{25}$ and platelet ice formation under near-coastal fast ice, which is related to the near-surface presence of sub-ice shelf melt water.

## 2. Regional setting

The areas investigated in this study include the southern Drake Passage, the continental shelves of the WAP and EAP (~60° S) and the more southerly located Amundsen and Weddell seas (~75° S; Fig. 1). The different study areas are all connected by the Antarctic Circumpolar Current (ACC), the Antarctic Coastal Current and the Weddell Gyre, respectively (Meredith et al., 2011; Rintoul et al., 2001).

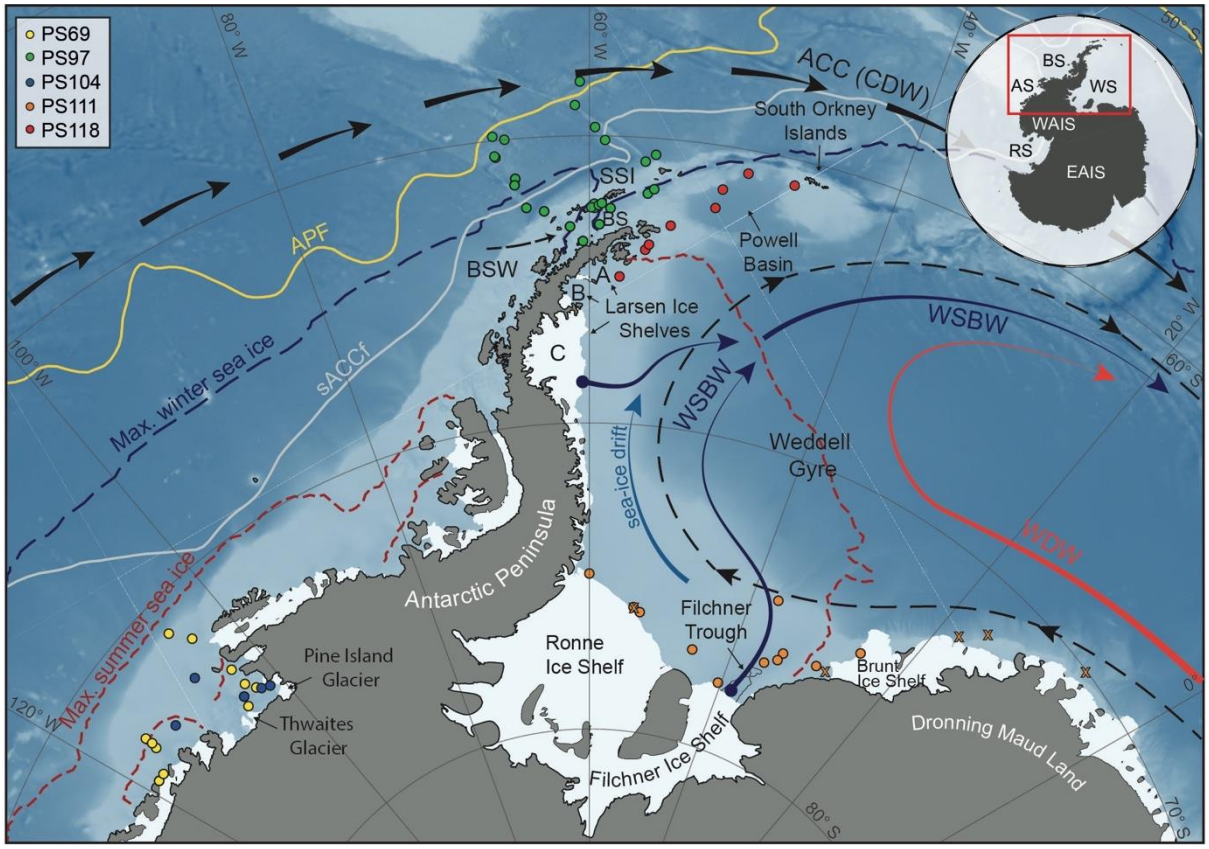


**Fig. 1:** Map of the study area (location indicated by red box in insert map) including all 41 sample locations (see different colored dots for individual RV *Polarstern* expeditions in the top left corner; for detailed sample information, see Table S1) and main oceanographic features. Maximum summer and winter sea-ice boundaries are marked by dashed red and blue line, respectively (Fetterer et al., 2016). The orange crosses in the Weddell Sea indicate samples with low biomarker concentrations close to detection limit, to which we assigned a $PIPSO_{25}$ value of 1. ACC: Antarctic Circumpolar Current, APF: Antarctic Polar Front, sACCf: southern Antarctic Circumpolar Current Front, SSI: South Shetland Islands, BS: Bransfield Strait, BSW: Bellingshausen Sea Water, CDW: Circumpolar Deep Water; WDW: Weddell Deep Water, WSBW: Weddell Sea Bottom Water (Mathiot et al., 2011; Orsi et al., 1995). Insert map shows grounded ice (*i.e.* without ice shelves) in black; WAIS: West Antarctic Ice Sheet, EAIS: East Antarctic Ice Sheet, RS: Ross Sea, AS: Amundsen Sea, BS: Bellingshausen Sea, WS: Weddell Sea. Background bathymetry derived from IBCSO data (Arndt et al., 2013).

The ACC, which is mainly composed of CDW and characterised by strong eastward flow, is the largest current system in the world and has its narrowest constriction in the Drake Passage. In the Bellingshausen Sea, the Amundsen Sea and along the WAP, where the ACC flows close to the continental shelf edge, CDW is upwelling onto the shelf and flows to the coast via bathymetric troughs, contributing to basal melt and retreat of marine-terminating glaciers and ice shelves (Cook et al., 2016; Jacobs et al., 2011; Jenkins and Jacobs, 2008; Klinck et al., 2004). In the Weddell Sea, the Weddell Gyre, a subpolar cyclonic circulation south of the ACC, deflects part of the ACC's CDW towards the south and turns it into Warm Deep Water (WDW; Fig. 1; Hellmer et al., 2016; Vernet et al., 2019). In close vicinity to the Filchner-Ronne and Larsen Ice Shelves, glacial meltwater as well as dense brines

153 released during sea-ice formation contribute to the formation of Weddell Sea Bottom Water (WSBW)
154 - a major precursor of Antarctic Bottom Water (Hellmer et al., 2016). Along the EAP coast wind and
155 currents force a northward drift of sea ice (Harms et al., 2001), which melts when reaching warmer
156 waters in the North and in Powell Basin (Vernet et al., 2019). At the northern tip of the Antarctic
157 Peninsula, colder and saltier Weddell Sea water masses branch off westwards into the Bransfield Strait,
158 where they encounter the well-stratified, warm, and fresh Bellingshausen Sea Water (BSW; Fig. 1),
159 which is entering the Bransfield Strait from the West (Sangrà et al., 2011).
160 Since 1978, satellite observations show strong seasonal and decadal changes in sea-ice cover aroundthe
161 Antarctic Peninsula, which are less pronounced in the Amundsen and Weddell seas (Vaughan et al.,
162 2003; Parkinson and Cavalieri, 2012). Mean monthly sea-ice concentrations (SIC) for austral winter
163 (JJA), spring (SON) and summer (DJF) reveal a permanently ice-free Drake Passage, while the WAP
164 and EAP shelf areas are influenced by a changing sea-ice cover throughout the year (Fig. 2a-c). For the
165 Amundsen and Weddell seas, satellite data reveal up to ~90 % sea-ice concentration during winter and
166 spring (Fig. 2a+b), and a minimum concentration of ~30 % during summer (Fig. 2c).

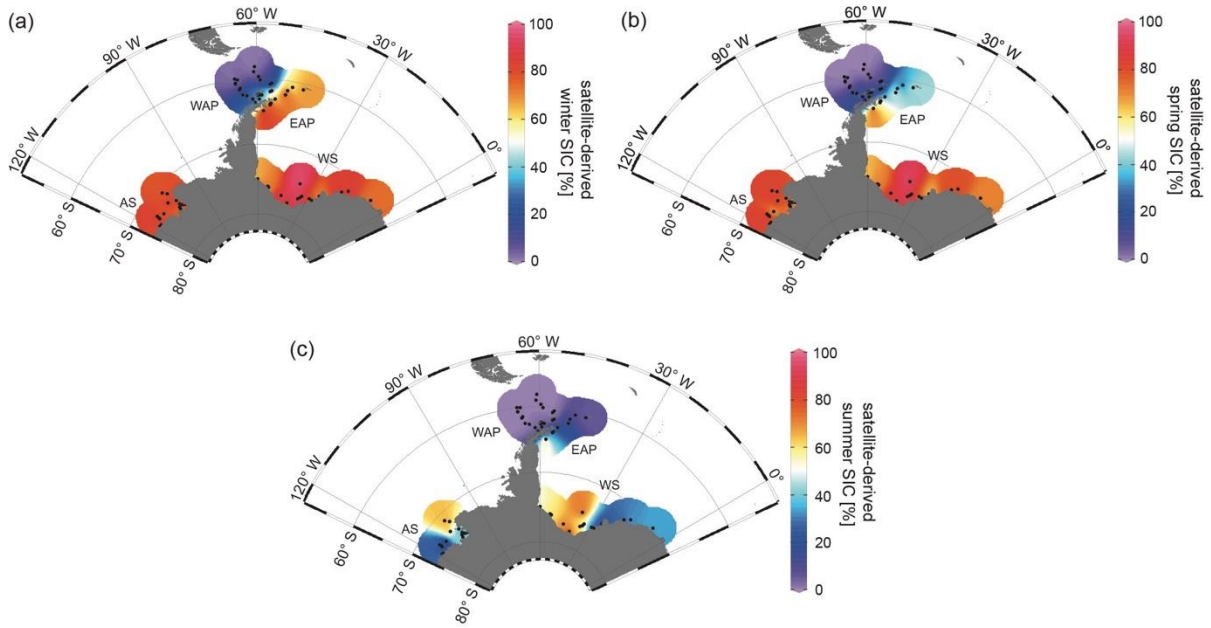


**Fig. 2:** Distribution of mean monthly satellite-derived sea-ice concentrations for (a) winter (JJA), (b) spring (SON) and (c) summer (DJF) in % (downloaded from the National Snow and Ice Data Center, NSIDC; Cavalieri et al., 1996). AS: Amundsen Sea, WAP: West Antarctic Peninsula, EAP: East Antarctic Peninsula, WS: Weddell Sea.

## 3. Material and methods

### 3.1 Sediment samples

We analysed a set of 41 surface sediment samples (0-1 cm subbottom depth) from different areas of the Southern Ocean (Fig. 1) retrieved by multicorers and giant box corers during RV *Polarstern* expeditions over the past 15 years. Sixteen surface sediment samples from the Amundsen Sea continental shelf were collected during expeditions PS69 in 2006 (Gohl, 2007) and PS104 in 2017 (Gohl, 2017). Twenty-five surface sediment samples from the southeastern and southwestern Weddell Sea continental shelf were collected during expeditions PS111 in 2018 (Schröder, 2018) and PS118 in 2019 (Dorschel, 2019). This new data set was complemented by data from 26 surface sediment samples collected in Bransfield Strait/WAP, which had been previously published by Vorrath et al. (2019).

### 3.2 Bulk sediment and organic geochemical analyses

The sediment material was freeze-dried and homogenized with an agate mortar and stored in glass vials at -20 °C before and after these initial preparation steps to avoid degradation of targeted molecular components. Total organic carbon (TOC) contents were measured on 0.1 g of sediment after removing inorganic carbon (total inorganic carbon, carbonates) with 500 µl 12 N hydrochloric acid. TOC contents were determined with a carbon-sulphur analyzer (CS 2000; Eltra) with standards for calibration being routinely measured before sample analysis and after every tenth sample (error ± 0.02 %).

Lipid biomarkers were extracted from the sediments (4 g for PS69 and PS104; 6 g for PS111 and PS118) by ultrasonication (3 x 15 min) using dichloromethane:methanol (3 x 6 ml for PS69 and PS104; 3 x 8 ml for PS111 and PS118; 2:1 v/v) as solvent. Prior to this step, the internal standards 7-hexylnonadecane (7-HND; 0.038 µg/sample for PS69 and PS104 and 0.057 µg/sample for PS111 and PS118), 5α-androstan-3-ol (1.04 µg/sample) and $C_{46}$ (0.98 µg/sample) were added to the sample for quantification of HBIs, sterols and GDGTs, respectively. Via open-column chromatography, with $SiO_2$ as stationary phase, fractionation of the extract was achieved by eluting the apolar fraction (HBIs) and the polar fraction (sterols and GDGTs) with 5 ml n-hexane and 5 ml DCM/MeOH 1:1, respectively. The polar fraction was subsequently split into two fractions (sterols and GDGTs) for further processing. The sterol fraction was silylated with 300 µl bis-trimethylsilyl-trifluoroacetamide (BSTFA; 2h at 60 °C).

Compound analyses of HBIs and sterols were carried out on an Agilent Technologies 7890B gas chromatograph (GC; fitted with a 30 m DB 1MS column; 0.25 mm diameter and 0.25 µm film thickness) coupled to an Agilent Technologies 5977B mass selective detector (MSD; with 70 eV constant ionization potential, ion source temperature of 230 °C). The GC oven was set to: 60 °C (3 min), 150 °C (rate: 15 °C/min), 320 °C (rate: 10 °C/min), 320 °C (15 min isothermal) for the analysis of hydrocarbons and to: 60 °C (2 min), 150 °C (rate: 15 °C/min), 320 °C (rate: 3 °C/min), 320 °C (20 min isothermal) for the analysis of sterols. Helium was used as carrier gas. The HBI and sterol compounds were identified by their GC retention times and mass spectra (Belt, 2018; Belt et al., 2000; Boon et al., 1979). Lipids were quantified by setting the individual, manually integrated, GC-MS peak area in relation to the peak area of the respective internal standard and normalization to the amount of extracted sediment. $IPSO_{25}$ and HBI trienes were quantified by relating their molecular ions ($IPSO_{25}$: m/z 348 and HBI trienes: m/z 346) to the fragment ion m/z 266 of the internal standard 7-HND (Belt, 2018). Sterols were quantified by comparing the molecular ion of the individual sterol with the molecular ion m/z 348 of the internal standard 5α-androstan-3-ol. Instrumental response factors for the target lipids were considered as recommended by Belt et al. (2014) and Fahl and Stein (2012). All biomarker concentrations were subsequently normalized to the TOC content of each sample to account for different depositional settings within the different study areas.

For calculating the phytoplankton-$IPSO_{25}$ ($PIPSO_{25}$) index, we used the equation introduced by Vorrath et al. (2019):

$$PIPSO_{25} = IPSO_{25} / (IPSO_{25} + (\text{phytoplankton marker x c})) \quad (1)$$

where c (c = mean $IPSO_{25}$/mean phytoplankton marker) is applied as a concentration balance factor to account for high concentration offsets between $IPSO_{25}$ and the phytoplankton biomarker (see Table S1 for c-factors of individual $PIPSO_{25}$ calculations).

Following the approach by Müller and Stein (2014) and Lamping et al. (2020), a $PIPSO_{25}$ value of 1 was assigned to samples with exceptionally low (at detection limit) concentrations of both biomarkers (see chapter 4.1.2). This comprises the five Weddell Sea samples PS111/13-2, /15-1, /16-3, /29-3 and /40-2 (marked as orange x in Fig. 1).

The GDGT fraction was dried under $N_2$, redissolved with 120 µl hexane:isopropanol (v/v 99:1) and then filtered using a polytetrafluoroethylene (PTFE) filter with a 0.45 µm pore sized membrane. GDGTs were measured using high performance liquid chromatography (HPLC; Agilent 1200 series HPLC system) coupled to an Agilent 6120 mass spectrometer (MS), operating with atmospheric pressure chemical ionization (APCI). The injection volume was 20 µl. For separating the GDGTs, a Prevail Cyano 3 µm column (Grace, 150 mm * 2.1 mm) was kept at 30 °C. Each sample was eluted isocratically for 5 min with solvent A = hexane/2-propanol/chloroform; 98:1:1 at a flow rate of 0.2 ml/min, then the volume of solvent B = hexane/2-propanol/chloroform; 89:10:1 was increased linearly to 10 % within 20 min and then to 100 % within 10 min. The column was back-flushed (5 min, flow 0.6 ml/min) after 7 min after each sample and re-equilibrated with solvent A (10 min, flow 0.2 ml/min). The APCI was set to the following: $N_2$ drying gas flow at 5 l/min and temperature to 350 °C, nebulizer pressure to 50 psi, vaporizer gas temperature to 350 °C, capillary voltage to 4 kV and corona current to +5 µA. Detection of GDGTs was achieved by means of selective ion monitoring (SIM) of $[M+H]^+$ ions (dwell time 76 ms). GDGT-0 (*m/z* 1302), GDGT-1 (*m/z* 1300), GDGT-2 (*m/z* 1298), GDGT-3 (*m/z* 1296) and crenarchaeol (*m/z* 1292) as well as brGDGT-III (*m/z* 1050), brGDGT-II (*m/z* 1036) and brGDGT-I (*m/z* 1022) were quantified by relating their molecular ions to the molecular ion *m/z* 744 of the internal standard $C_{46}$-GDGT. The late eluting hydroxylated GDGTs (OH-GDGT-0, OH-GDGT-1 and OH-GDGT-2 with *m/z* 1318, 1316 and 1314, respectively) were quantified in the scans (*m/z* 1300, 1298, 1296) of their related GDGTs, as described by Fietz et al. (2013).

$TEX^{L}_{86}$ values and their conversion into SOTs were determined following Kim et al. (2012):

$$TEX^{L}_{86} = LOG\frac{[GDGT-2]}{[GDGT-1]+[GDGT-2]+[GDGT-3]}, \quad (2)$$

$$SOT^{TEX}\,[°C] = 50.8 \text{ x } TEX^{L}_{86} + 36.1. \quad (3)$$

Temperature calculations based on OH-GDGTs were carried out according to Lü et al. (2015):

$$RI - OH' = \frac{[OH-GDGT-1]+2 \text{ x } [OH-GDGT-2]}{[OH-GDGT-0]+[OH-GDGT-1]+[OH-GDGT-2]}, \quad (4)$$

$$SST^{OH}\,[°C] = RI - OH' - 0.1/0.0382\,. \quad (5)$$

To determine the relative influence of terrestrial organic matter input, the Branched Isoprenoid Tetraether (BIT)-index was calculated following Hopmans et al. (2004):

$$\mathrm{BIT} = \frac{[\mathrm{brGDGT\text{-}I}]+[\mathrm{brGDGT\text{-}II}]+[\mathrm{brGDGT\text{-}III}]}{[\mathrm{Chrenarchaeol}]+[\mathrm{brGDGT\text{-}I}]+[\mathrm{brGDGT\text{-}II}]+[\mathrm{brGDGT\text{-}III}]}. \quad (6)$$

### 3.3 Numerical model

#### 3.3.1 Model description

AWI-ESM2 is a state-of-the-art coupled climate model developed by Sidorenko et al. (2019) which comprises an atmospheric component ECHAM6 (Stevens et al., 2013) as well as an ocean-sea ice component FESOM2 (Danilov et al., 2017). The atmospheric module ECHAM6 is the most recent version of the ECHAM model developed at the Max Planck Institute for Meteorology (MPI) in Hamburg. The model is branched from an early release of the European Center (EC) for Medium Range Weather Forecasts (ECMWF) model (Roeckner et al., 1989). ECHAM6 dynamics is based on hydrostatic primitive equations with traditional approximation. We used a T63 Gaussian grid with a spatial resolution of about 1.9 x 1.9 degree (1.9 ° or 210 km). There are 47 vertical layers in the atmosphere.

Momentum transport arising from boundary effects is configured using the subgrid orography scheme as described by Lott (1999). Radiative transfer in ECHAM6 is represented by the method described in Iacono et al. (2008). ECHAM6 also contains a Land-Surface Model (JSBACH) which includes 12 functional plant types of dynamic vegetation and 2 bare-surface types (Loveland et al., 2000; Raddatz et al., 2007). The ice-ocean module in AWI-ESM2 is based on the finite volume discretization formulated on unstructured meshes. The multi-resolution for the ocean is up to 15 km over polar and coastal regions, and 135 km for far-field oceans, with 46 uneven vertical depths. The impact of local dynamics on the global ocean is related to a number of FESOM-based studies (Danilov et al., 2017). The multi-resolution approach advocated by FESOM allows to explore the impact of local processes on the global ocean with moderate computational effort (Danilov et al., 2017). AWI-ESM2 employs the OASIS3-MCT coupler (Valcke, 2013) with an intermediate regular exchange grid. Mapping between the intermediate grid and the atmospheric/oceanic grid is handled with bilinear interpolation. The atmosphere component computes 12 air–sea fluxes based on four surface fields provided by the ocean module FESOM2. AWI-ESM2 has been validated under modern climate conditions (Sidorenko

et al., 2019) and has been applied for marine radiocarbon concentrations (Lohmann et al., 2020), the latest Holocene (Vorrath et al., 2020), and the Last Interglacial (Otto-Bliesner et al., 2021).

#### 3.3.2 Experimental design

One transient experiment was conducted using AWI-ESM2, which applied the boundary conditions, including orbital parameters and greenhouse gases. Orbital parameters are calculated according to Berger (1978), and the concentrations of greenhouse gases are taken from ice-core records and measurements of recent firn air and atmospheric samples (Köhler et al., 2017). The model was initialized from a 1,000-year spin-up run under mid-Holocene (6,000 before present, BP) boundary conditions as described by Otto-Bliesner et al. (2017). In our modeling strategy, we follow Lorenz and Lohmann (2004) and use the climate condition from the mid-Holocene spin-up run as the initial state for the subsequent transient simulation covering the period from 6,000 BP to 2014 Common Era (CE). In the present study we derived seasonal SIC, SSTs and SOTs in the study areas from a segment of the transient experiment (1950-2014 CE). Topography including prescribed ice sheet configuration was kept constant in our transient simulation. All model data are provided in Table S2.

### 3.4. Satellite SIC and SSTs

Satellite sea-ice data were derived from Nimbus-7 SMMR and DMSP SSM/I-SSMIS passive microwave data and downloaded from the National Snow and Ice Data Center (NSIDC; Cavalieri et al., 1996). The sea-ice data represent mean monthly SIC, which are expressed to range from 0 % to 100 % and are averaged over a period of the beginning of satellite observations in 1978 CE to the individual year of sample collection. The monthly mean SIC were then split into different seasons: winter (JJF), spring (SON) and summer (DJF) (Fig. 2a-c), and these data are considered to represent the recent mean state of sea-ice coverage. All satellite data are provided in Table S3.

Modern annual mean SSTs and SOTs were derived from the World Ocean Atlas 2013 and represent averaged values for the years 1955-2012 CE (WOA13; Locarnini et al., 2013).

## 4. Results and discussion

In the following, we first present and discuss the biomarker data generated for this study from North (Antarctic Peninsula) to South (Amundsen and Weddell seas) and draw conclusions about the environmental settings deduced from the data set. In regard to the phytoplankton-derived biomarkers, we focus on the significance of HBI Z-triene and brassicasterol, because the HBI E-triene and dinosterol data, which are presented in the supplementary material (Fig. S1), show very similar patterns. All biomarker data are provided in Table S1 and are available from the PANGAEA data repository (DOI in prep.). For the discussion of the target environmental variables, *i.e.* $PIPSO_{25}$-based sea-ice and GDGT-derived ocean temperature estimates, satellite, instrumental and model data are considered. In section 5, we further address potential caveats in biomarker-based environmental reconstructions that need to be taken into account when applying these proxies.

### 4.1 TOC content, HBIs and sterols in Antarctic surface sediments

TOC contents in marine sediments are often viewed as an indicator for primary productivity in surface waters (Meyers, 1997). However, we are aware that additional factors, such as different water depths and depositional regimes, may exert control on sedimentary TOC as well. The TOC contents of the investigated surface samples are lowest in Drake Passage with values around 0.12-0.54 % and increase from northwest to southeast into Bransfield Strait, where they range from 0.59 to 1.06 % (Fig. 3a; WAP). Along the EAP, higher TOC contents (0.57-0.86 %) prevail around the former Larsen A Ice Shelf and north of James Ross Island but they decrease towards Powell Basin (0.22-0.37 %) and then increase to 0.50 % around the South Orkney Islands, which may point to elevated productivity or enhanced supply of reworked terrigenous organic matter in this area (Fig. 3a; EAP).

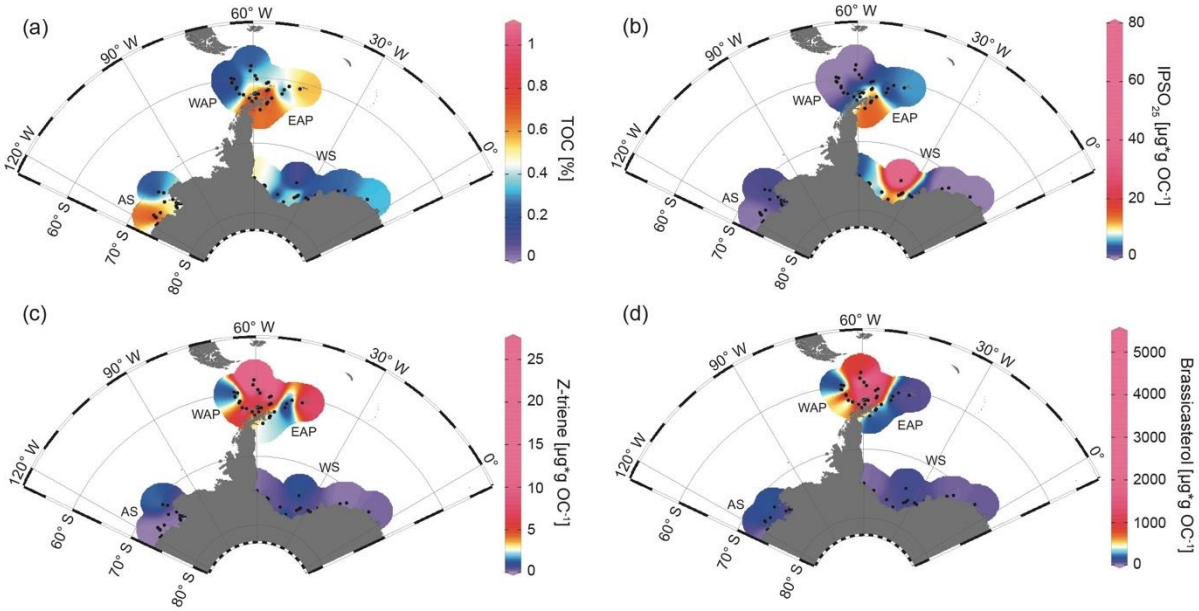


**Fig. 3:** Distribution of (a) TOC [%], (b) $IPSO_{25}$, (c) Z-triene and (d) brassicasterol in surface sediment samples. Sample locations are marked as black dots. Concentrations of biomarkers [µg*g $OC^{-1}$] were normalized to the TOC content of each sample. AS: Amundsen Sea, WAP: West Antarctic Peninsula, EAP: East Antarctic Peninsula, WS: Weddell Sea.

At the WAP, concentrations of the sea-ice biomarker $IPSO_{25}$ increase from northwest to southeast. $IPSO_{25}$ is absent in samples from the permanently ice-free Drake Passage and increases towards the continental slope and the seasonally ice-covered shelf (0.37-17.81 µg*g $OC^{-1}$; Fig. 3b; Vorrath et al., 2019). Highest $IPSO_{25}$ concentrations are observed in samples of the northern Bransfield Strait. Here, the inflow of waters from the Weddell Sea transports sea ice into Bransfield Strait (Vorrath et al., 2019). Elevated $IPSO_{25}$ concentrations are also observed at the seasonally sea-ice covered EAP, where relatively high concentrations of the sea-ice biomarker prevail in samples located in the area of the former Larsen A Ice Shelf and north of James Ross Island (12.59-17.74 µg*g $OC^{-1}$; Fig. 3b). Because these locations are influenced by the northward drift of sea ice within the Weddell Gyre (Fig. 1), the elevated $IPSO_{25}$ concentrations could also result from sea ice advected from the southern Weddell Sea. We suggest that the decrease of $IPSO_{25}$ concentrations towards the Powell Basin and the South Orkney Islands (0.59-5.36 µg*g $OC^{-1}$; Fig. 3b) is connected to warmer ocean temperatures in the North and reduced sea-ice cover during spring.

Concentrations of the phytoplankton biomarker HBI Z-triene around the Antarctic Peninsula are highest in eastern Drake Passage and along the WAP continental slope (where $IPSO_{25}$ is absent) and decrease

in Bransfield Strait (0.33-26.86 µg*g $OC^{-1}$; Fig. 3c; Vorrath et al., 2019). Elevated HBI Z-triene concentrations have, so far, been detected in surface waters along the sea-ice edge (Smik et al., 2016) and hence were suggested to be a proxy for marginal ice zone conditions (Belt et al., 2015; Collins et al., 2013; Schmidt et al., 2018). Vorrath et al. (2019), however, relate the high concentrations of HBI Z-triene at the northernmost stations in the permanently ice-free eastern Drake Passage to their proximity to the Antarctic Polar Front. Here, productivity of the source diatoms of HBI-trienes (*e.g.*, *Rhizosolenia* spp.; Belt et al., 2017) may be enhanced by meander-induced upwelling leading to increased nutrient flux to surface waters (Moore and Abbott, 2002). Since Cardenas et al. (2019) document only minor abundances of *Rhizosolenia* spp. in seafloor surface sediments from this area, we assume that HBI-trienes might also be biosynthesized by other diatom taxa. Moderate concentrations along the continental slope of the WAP and in Bransfield Strait were associated with elevated inflow of warm BSW which leads to a retreating sea-ice margin during spring and summer (for more details, see Vorrath et al., 2019; 2020). Samples from the EAP shelf and Powell Basin are characterised by relatively low HBI Z-triene concentrations (Fig. 3c; 0.1-2.37 µg*g $OC^{-1}$) that decrease from southwest to northeast, whereas the northernmost sample closest to the South Orkney Islands is characterized by an elevated HBI Z-triene concentration of ~8.49 µg*g $OC^{-1}$ (Fig. 3c; EAP). This relatively high concentration may be related to an "Island Mass Effect", coined by Doty and Oguri (1956), which refers to increased primary production around oceanic islands in comparison to surrounding waters. Nolting et al. (1991) found extraordinarily high dissolved iron levels (as high as 50-60 nM) on the South Orkney shelf, while Nielsdóttir et al. (2012) observed enhanced iron and Chl *a* concentrations in the vicinity of the South Orkney Islands. These authors explain the increased dissolved iron levels with input from seasonally retreating sea ice, which is recorded by satellites (Fig. 2a-c) and probably leads to substantial annual phytoplankton blooms, which may also cause the elevated TOC content in the corresponding seafloor sediment sample (Fig. 3a). Alternatively, remobilization of shelf sediments or vertical mixing of iron-rich deep waters, leading to high iron contents in surface waters, may stimulate primary productivity (Blain et al., 2007; de Jong et al., 2012). However, it remains unclear why the brassicasterol concentration is distinctly low in this sample, and we assume that different environmental preferences of the source organisms may account for this. In Drake Passage and along the EAP, brassicasterol

displays a similar pattern as HBI Z-triene, with relatively high concentrations (more than 2 orders of magnitudes) ranging from 1.86 to 5017.44 µg*g $OC^{-1}$ (Fig. 3d).

In the Weddell Sea, TOC contents are generally low (< 0.4 %), with slightly elevated values in the West (up to 0.50 %) and right in front of the Filchner Ice Shelf (up to 0.52 %; Fig. 3a). The Amundsen Sea is characterized by slightly higher TOC contents, with concentrations of up to 0.91 % in the West and lower values in the East (0.33 %; Fig. 3a; AS).

In the samples from the Amundsen and Weddell seas, that both are dominated by strong winter sea-ice cover lasting until spring (Fig. 2a-c), all three biomarkers are present in low concentrations only. An exception are the samples located in front of the Filchner Ice Shelf with significantly higher concentrations of $IPSO_{25}$ (7.09-73.87 µg*g $OC^{-1}$; Fig. 3b; WS). Concentrations of $IPSO_{25}$ on the Amundsen Sea shelf are relatively low (0.04-3.3 µg*g $OC^{-1}$), with slightly higher values observed in the north-east (Fig. 3b; AS). HBI Z-triene concentrations are also very low, but slightly higher in Filchner Trough (0.04-1 µg*g $OC^{-1}$) and at more distal locations on the northeastern Amundsen Sea shelf (0.01-1.88 µg*g $OC^{-1}$; Fig. 3c). Brassicasterol generally shows a similar pattern as HBI Z-triene, with concentrations varying between 1.86 and 220.54 µg*g $OC^{-1}$ (Fig. 3d; for HBI E-triene and dinosterol distribution, see Fig. S1).

### 4.2 Combining individual biomarker records: the $PIPSO_{25}$ index

The $PIPSO_{25}$ index combines the relative concentrations of $IPSO_{25}$ and a selected phytoplankton biomarker, such as HBI-trienes and sterols, as indicator for an open-ocean environment (Vorrath et al., 2019). The combination of both end members (sea ice vs. open-ocean) prevents misleading interpretations regarding the absence of $IPSO_{25}$ in the sediments, which can be the result of two entirely different scenarios. Under heavy/perennial sea-ice coverage, the thickness of sea ice hinders light penetration, thereby limiting the productivity of algae living in basal sea ice (Hancke et al., 2018). This scenario can cause the absence of both phytoplankton and sea-ice biomarkers in the sediment. The other scenario depicts a permanently open ocean, where the sea-ice biomarker is absent as well, but here the phytoplankton biomarkers are present in variable concentrations (Müller et al., 2011). The presence of both biomarkers in the sediment is indicative of seasonal sea-ice coverage and/or the occurrence of

396 stable sea-ice margin conditions, promoting biosynthesis of both biomarkers (Müller et al., 2011). We
397 here distinguish between $P_ZIPSO_{25}$ and $P_BIPSO_{25}$ using HBI Z-triene and brassicasterol as
398 phytoplankton biomarker, respectively (Fig. 4a+b; for $PIPSO_{25}$ values based on HBI E-triene and
399 dinosterol see Table S1 and Fig. S2).

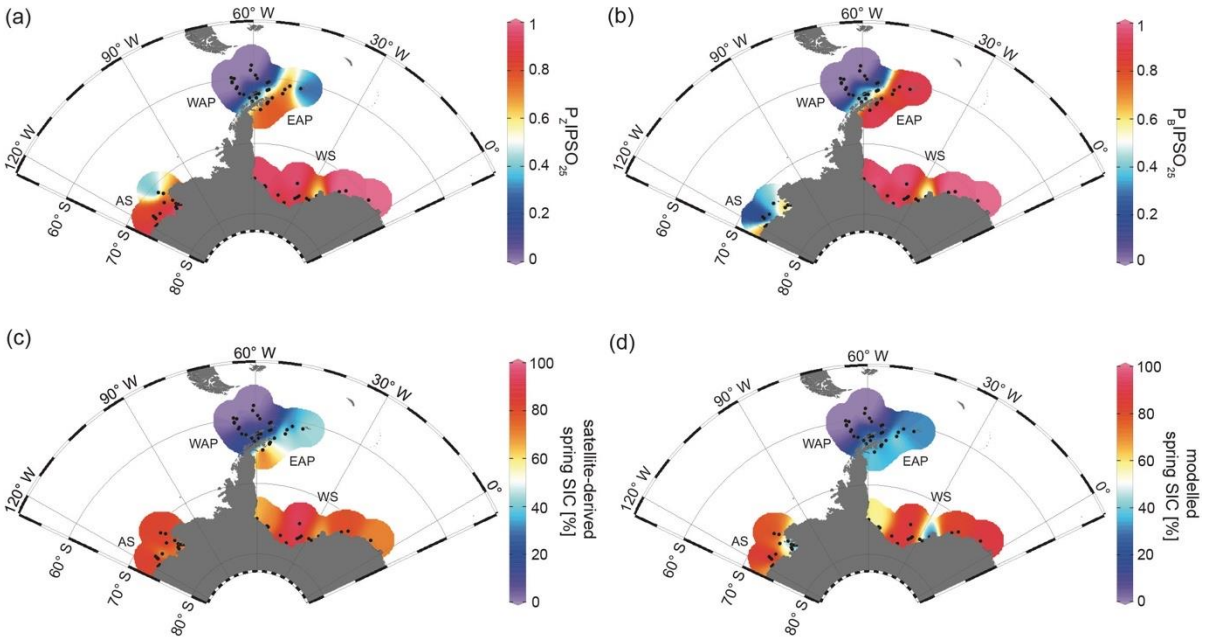


**Fig. 4:** Distribution of the sea-ice index $PIPSO_{25}$ in surface sediment samples, with (a) $P_ZIPSO_{25}$ based on Z-triene and (b) $P_BIPSO_{25}$ based on brassicasterol, (c) satellite-derived spring SIC [%] and (d) modelled spring SIC [%]. AS: Amundsen Sea, WAP: West Antarctic Peninsula, EAP: East Antarctic Peninsula, WS: Weddell Sea.

400 Both $PIPSO_{25}$ indices are 0 in the predominantly ice-free Drake Passage and increase towards southeast
401 to intermediate values on the WAP slope and around the South Shetland Islands, reflecting increased
402 influence of marginal sea-ice cover towards the coast (0.02-0.70; Vorrath et al., 2019). At the seasonally
403 sea-ice covered EAP, $P_ZIPSO_{25}$ values reach 0.84, while lower values of around 0.25 are observed close
404 to the South Orkney Islands, which is caused by the elevated HBI Z-triene concentrations at the stations
405 there (Fig. 3c; EAP). The $P_BIPSO_{25}$ index exhibits even higher values of up to 0.98 at the
406 EAP/northwestern Weddell Sea. These elevated $PIPSO_{25}$ indices align well with the significant
407 northward sea-ice drift within the Weddell Gyre, which leads to prolonged sea-ice cover along the EAP.
408 In samples from the southern Weddell Sea, both $PIPSO_{25}$ indices show a similar pattern with high values
409 up to 0.9, and slightly lower values in front of the Brunt Ice Shelf (0.6; Fig. 4a+b). Very low
410 concentrations (close to detection limit) of both biomarkers in samples from the continental shelf off

411 Dronning Maud Land (Fig. 1) result in low $PIPSO_{25}$ values, strongly underestimating the sea-ice cover
412 in this area, where satellite-derived sea-ice data document severe seasonal sea-ice cover (Fig. 2). As
413 previously mentioned, we followed the approach by Müller and Stein (2014) and Lamping et al. (2020)
414 by assigning a maximum $PIPSO_{25}$ value of 1 to these samples to circumvent misleading interpretations
415 and aid visualisation.
416 The intermediate $PIPSO_{25}$ value (~0.51) derived for one sample collected in front of the Brunt Ice Shelf
417 points to a less severe sea-ice cover in that area. A possible explanation for the relatively low $PIPSO_{25}$
418 value is the presence of a coastal polynya that has been reported by Anderson (1993) and which is
419 further supported by Paul et al. (2015). These authors note that the sea-ice area around the Brunt Ice
420 Shelf is the most active in the southern Weddell Sea, with an annual average polynya area of 3516 ±
421 1420 km². Interestingly, the reduced SIC here is also captured by our model (see section 4.3).
422 $PIPSO_{25}$ values in the Amundsen Sea point to different scenarios. The $P_ZIPSO_{25}$ index varies around
423 0.9, with only the easterly, more distal samples having lower values between 0.3 and 0.6 (Fig. 4a). The
424 $P_BIPSO_{25}$ index generally has lower values, ranging from 0.6 in the coastal area to 0.2 in the more distal
425 samples (Fig. 4b). This difference between $P_ZIPSO_{25}$ and $P_BIPSO_{25}$ may be explained by the different
426 source organisms biosynthesizing the individual phytoplankton biomarkers. While the main
427 origin of HBI-trienes seems to be restricted to diatoms (Belt et al., 2017), brassicasterol is known to
428 be produced by several algal groups that are adapted to a wider range of sea surface conditions
429 (Volkman, 2006; see section 5.2).
430
431 ### 4.3 Biomarker-based sea ice estimates vs. satellite and model data
432 The main ice algae bloom in the Southern Ocean occurs during spring, when solar insolation and air
433 temperatures/SSTs increase and sea ice starts to melt, which results in the release of nutrients and
434 stratification of the water column stimulating the productivity of photosynthesizing organisms (Arrigo,
435 2017; Belt, 2018). The sea-ice biomarker $IPSO_{25}$ is hence commonly interpreted as a spring sea-ice
436 indicator, which is why, in the following, we compare the biomarker-based sea-ice reconstructions to
437 satellite-derived and modelled spring SIC. $IPSO_{25}$ concentrations in the surface sediments around the

Antarctic Peninsula exhibit similar trends as the satellite-derived and modelled SIC (Figs. 3+4), while they differ significantly in the Amundsen and Weddell seas, where high SIC are recorded by satellites and the model but $IPSO_{25}$ is present in low concentrations. The low $IPSO_{25}$ concentrations in these areas highlight the uncertainty, when considering $IPSO_{25}$ as a sea-ice proxy alone, since such low concentrations are not only observed under open water conditions, but also under severe sea-ice cover. In the Amundsen and Weddell seas, the low $IPSO_{25}$ concentrations are the result of the latter, where limited light availability hinders ice algae growth, leading to an underestimation of sea-ice cover. Accordingly, we note a weak correlation between $IPSO_{25}$ data and satellite SIC ($R^2 = 0.19$; Fig. 5a). As stated above, the combination of $IPSO_{25}$ and a phytoplankton marker may prevent this ambiguity. The higher sea-ice concentrations in the Amundsen and Weddell seas are better reflected by maximum $P_ZIPSO_{25}$ values than by $IPSO_{25}$ alone. However, we note that the $P_ZIPSO_{25}$ index apparently does not resolve SICs higher than 50 % (see Fig. S3), which may indicate a threshold (here ~50 % SIC) where the growth of the HBI-triene and $IPSO_{25}$ producing algae is limited.

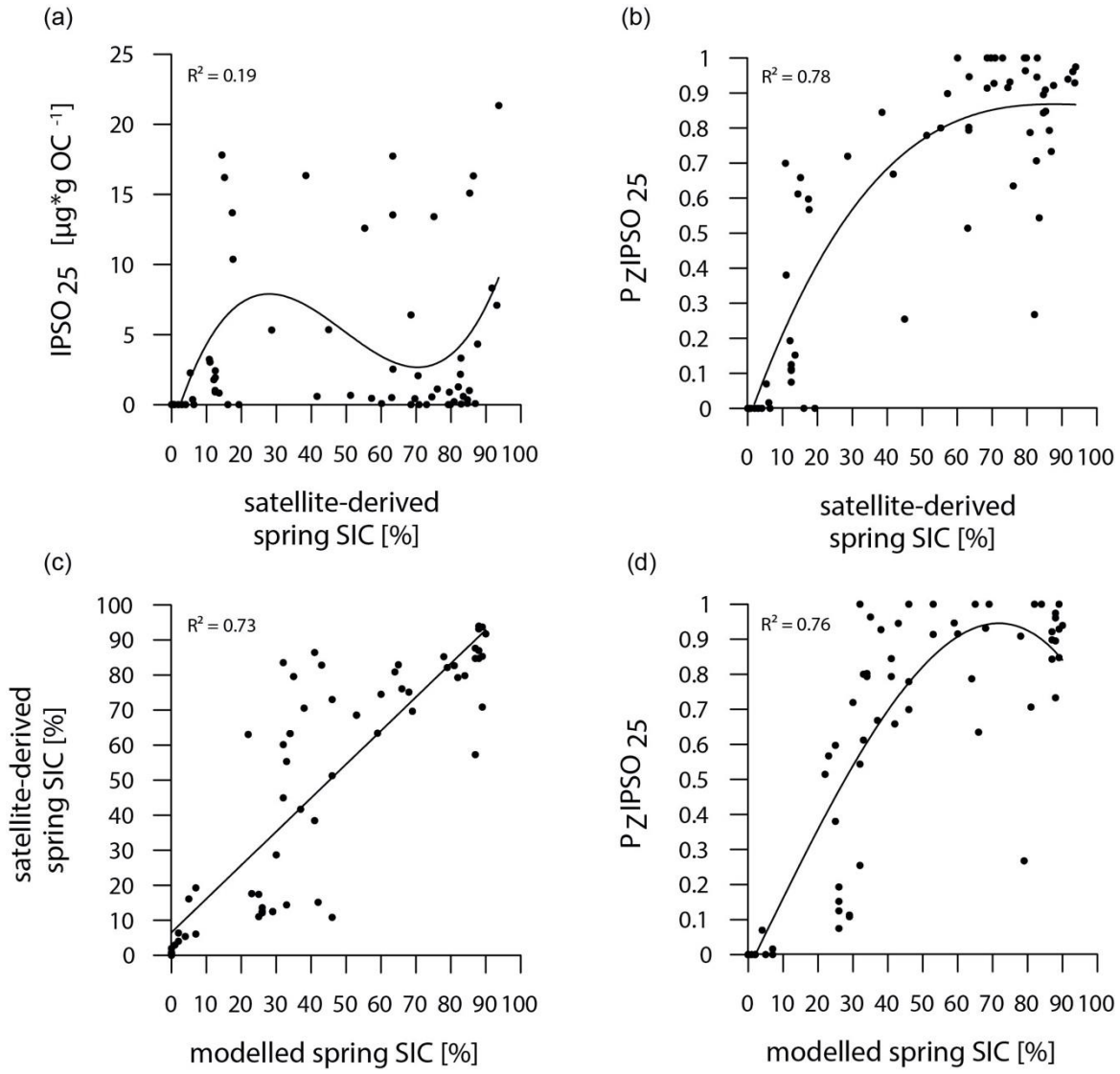


**Fig. 5:** Correlations of (a) $IPSO_{25}$ concentrations vs. satellite-derived spring SIC, (b) $P_ZIPSO_{25}$ values vs. satellite-derived spring SIC, (c) satellite-derived spring SIC vs. modelled spring SIC and (d) $P_ZIPSO_{25}$ values vs. modelled spring SIC. Coefficients of determination ($R^2$) are given for the respective regression lines.

In general, however, the $P_ZIPSO_{25}$ values correlate much better with satellite and modelled SIC ($R^2$ = 0.78 and $R^2$ = 0.76, respectively; Fig. 5b+d) than $IPSO_{25}$ concentrations. Correlations of satellite and model data with $PIPSO_{25}$ calculated using the HBI E-triene, brassicasterol and dinosterol, respectively, are also positive but less significant (Fig. S4), and we hence focus the discussion on $P_ZIPSO_{25}$.The AWI-ESM2-derived spring SICs correctly display the permanently ice-free Drake Passage and the northwest-southeast increase in sea-ice cover from the WAP continental slope towards Bransfield Strait (Fig. 4d). The model, however, significantly underestimates the elevated sea-ice concentrations (up to 70 %) in front of the former Larsen Ice Shelf A and east of James Ross Island at the EAP observed in satellite

data. In the Amundsen and Weddell seas, the model predicts heavy sea-ice cover (~90 %), only slightly underestimating the sea-ice cover at the near-coastal sites in front of Pine Island Glacier and Ronne Ice Shelf. Interestingly, modelled SIC in front of Brunt Ice Shelf is as low as ~45 % (Fig. 4d+e), corresponding well with the reduced $P_ZIPSO_{25}$ value of ~0.51. This may reflect the polynya conditions in that region documented by Anderson (1993) and Paul et al. (2015). Overall, we note that modelled modern SICs correlate well with satellite data ($R^2 = 0.73$; Fig. 5c) and $P_ZIPSO_{25}$ values ($R^2 = 0.76$; Fig. 5d), while we observe weaker correlations between modelled paleo-SICs and $P_ZIPSO_{25}$ values (Fig. S5; see section 5.1).

### 4.4 $TEX^L_{86}$- and RI-OH'-derived ocean temperatures

For a critical appraisal of the applicability and reliability of GDGT indices as temperature proxies in polar latitudes, we here focus on the $TEX^L_{86}$ proxy by Kim et al. (2012), which potentially reflects SOTs, and the RI-OH' proxy by Lü et al. (2015), which is assumed to reflect SSTs. The reconstructions are believed to represent annual mean ocean temperatures (for correlations of $TEX^L_{86}$-derived SOTs with WOA spring and winter SOTs, see Fig. S6). In all samples, the BIT-index (Eq. 6) is <0.3, indicating no significant impact of terrestrial input of organic material on the distribution of GDGTs and hence their reliability as temperature proxy. RI-OH'-derived temperatures and $TEX^L_{86}$-derived SOTs both show a similar pattern, but different temperatures ranges between -2.62 to +4.67 °C and -2.38 to +8.75 °C, respectively (Fig. 6a+b). At the WAP, RI-OH'- as well as $TEX^L_{86}$-derived temperatures increase northwestwards across the Antarctic continental slope and into the permanently ice-free Drake Passage, which are influenced by the ACC and relatively warm CDW (Orsi et al., 1995; Rintoul et al., 2001). Temperatures decrease towards Bransfield Strait and the EAP, which are influenced by seasonal sea-ice cover and relatively cold water from the Weddell Sea that branches off the Weddell Gyre (Collares et al., 2018; Thompson et al., 2009). At the EAP, a southwestward decrease is observed, with

relatively low temperatures at the former Larsen A Ice Shelf and higher temperatures recorded in Powell Basin and around the South Orkney Islands (Fig. 6a+b).

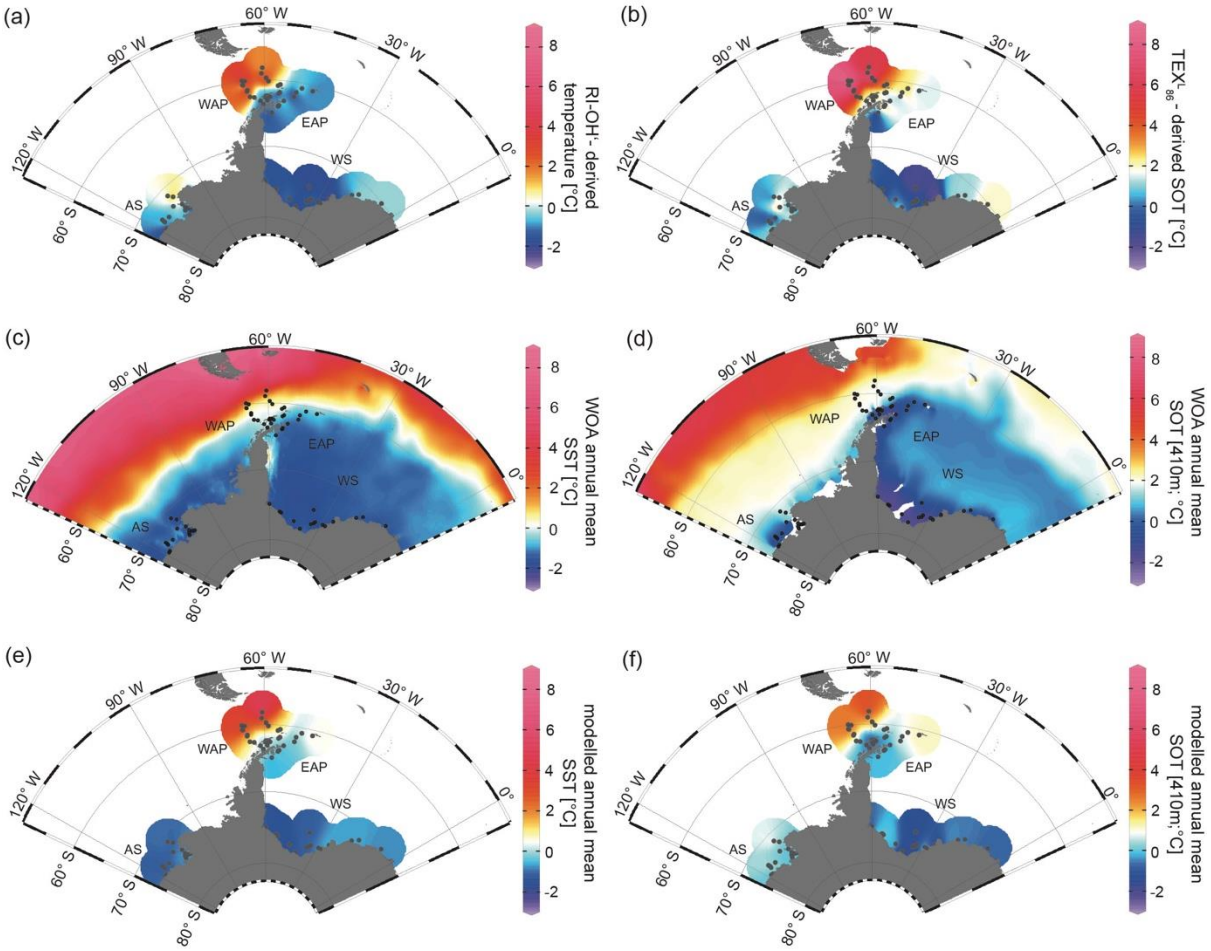


**Fig. 6:** Annual mean temperature distributions with (a) RI-OH´-derived temperature, (b) $TEX^{L}_{86}$-derived SOT, (c) WOA13 SST (Locarnini et al., 2013), (d) WOA13 SOT (410 m; Locarnini et al., 2013), (e) modelled SST and (f) modelled SOT (410 m) in °C. AS: Amundsen Sea, WAP: West Antarctic Peninsula, EAP: East Antarctic Peninsula, WS: Weddell Sea.

In the Amundsen and Weddell seas further south, reconstructed temperatures are generally lower than around the Antarctic Peninsula. Samples from the Weddell Sea display a temperature decrease from east to west, which may reflect the route of eddies in the northeastern Weddell Gyre. These eddies carry relatively warm, salty CDW westward along the southern limb of the Weddell Gyre, where it becomes WDW (Vernet et al., 2019). Coldest $TEX^{L}_{86}$ and RI-OH' temperatures (<0 °C) at sites along the Filchner-Ronne Ice Shelf front may be further linked to the presence of cold precursor water masses for WSBW.

With regard to ongoing discussions, whether GDGT-based temperature reconstructions represent SSTs or SOTs (Kalanetra et al., 2009; Kim et al., 2012; Park et al., 2019), we here compare our RI-OH' and $TEX^{L}_{86}$-derived temperatures with surface and subsurface temperature data obtained by in-situ measurements and modelling (Fig. 6c-f). Comparison of GDGT-derived temperatures with WOA13 temperatures from different water depths reveals the most significant correlation for a water depth of 410 m (for respective correlations, see Fig. S7). When discussing instrumental and modelled SOTs, we hence refer to 410 m water depth.

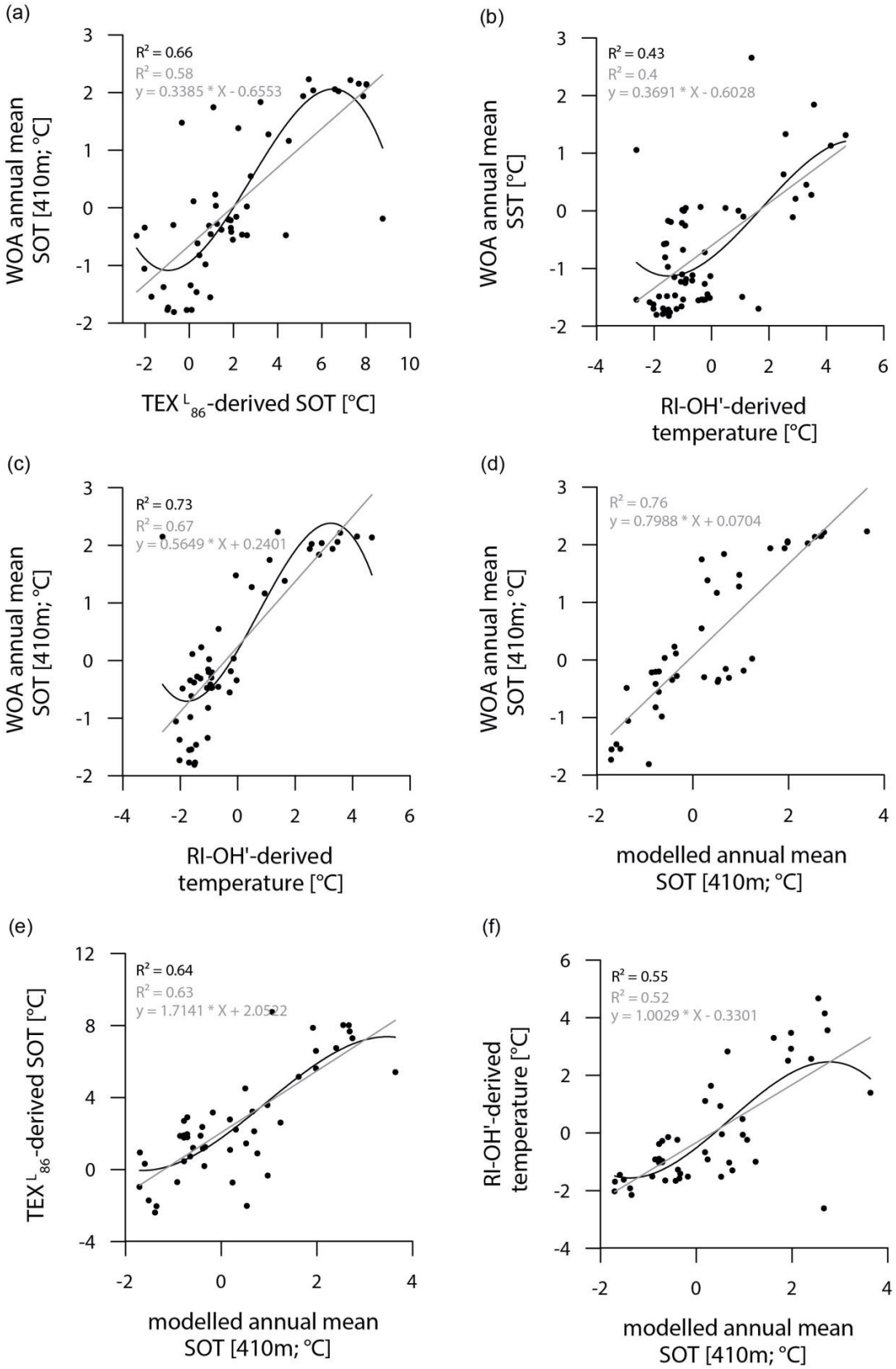


**Fig. 7:** Correlations of (a) WOA annual mean SOT (410 m) vs. $TEX^{L}_{86}$-derived SOT, (b) WOA annual mean SST vs. RI-OH'-derived temperature, (c) WOA annual mean SOT (410 m) vs. RI-OH'-derived temperature, (d) WOA annual mean SOT (410 m) vs. modelled annual mean SOT (410 m), (e) $TEX^{L}_{86}$-derived SOT vs. modelled annual mean SOT (410 m), (f) RI-OH'-derived temperature vs. modelled annual mean SOT (410 m) in °C. Coefficients of determination ($R^2$) are given for the respective regression lines.

While the correlation between $TEX^{L}_{86}$-derived SOTs and instrumental SOTs is reasonably good (Fig. 7a; $R^2$ = 0.66), also supporting a subsurface origin for the $TEX^{L}_{86}$ proxy, we note a significant overestimation of SOTs by up to 6 °C in Drake Passage (Fig. S8). This warm-biased $TEX^{L}_{86}$ signal is a known caveat and is, among others, assumed to be connected to GDGTs produced by deep-dwelling Euryarchaeota (Park et al., 2019), which have been reported in CDW (Alonso-Sáez et al., 2011) and in deep waters at the Antarctic Polar Front (López-García et al., 2001). Maximum $TEX^{L}_{86}$-based SOTs of 5 °C - 8 °C in central Drake Passage (Fig. 6b), however, distinctly exceed the common temperature range of CDW (0-2 °C). Interestingly, $TEX^{L}_{86}$-derived SOTs in the colder regions of the Amundsen and Weddell seas relate reasonably well to instrumental temperatures and are only slightly warm-biased (Fig. S8). Correlations between RI-OH'-derived temperatures and instrumental SSTs are weak ($R^2$ = 0.43; Fig. 7b). Recently, Liu et al. (2020) concluded in their study on surface sediments from Prydz Bay (East Antarctica), that also the RI-OH' index holds promise as a tool to reconstruct SOTs rather than SSTs. When correlating our RI-OH'-derived temperatures with instrumental SOTs, we similarly find a high correlation ($R^2$ = 0.73; Fig. 7c), hence supporting this hypothesis. We further note that the RI-OH' temperature range is much more realistic than the $TEX^{L}_{86}$ range. This suggests that the addition of OH-isoGDGTs in the temperature index is a promising step towards reliable high latitude temperature reconstructions and may improve our understanding of the temperature responses of archaeal membranes in Southern Ocean waters (Fietz et al., 2020; Park et al., 2019). Clearly, more data – ideally obtained from sediment traps, seafloor surface sediment samples and longer sediment cores – and calibration studies will help to further elucidate the applicability of the RI-OH' and $TEX^{L}_{86}$ temperature reconstructions.

Similar to the model-derived sea-ice data, we also evaluate the model's performance in depicting ocean temperatures (Fig. 6e+f). Modelled annual mean SSTs and SOTs are highest (with up to 5 °C and 3 °C, respectively) in the permanently ice-free Drake Passage, which is influenced by the relatively warm ACC. Lower SSTs are predicted for the Antarctic Peninsula continental slope and Bransfield Strait (~0.5 to 1 °C), coinciding with the increase in the duration of seasonal sea-ice cover in that area. At the EAP/northwestern Weddell Sea, modelled SSTs as well as SOTs increase from southwest to northeast

towards Powell Basin. In the Amundsen and Weddell seas, annual mean SSTs are negative, with temperatures ranging from -1 to -0.5 °C, while SOTs are positive in the Amundsen Sea and negative in the Weddell Sea. Overall, we note that modelled SOTs reflect instrumental SOTs reasonably well ($R^2$ = 0.76; Fig. 7d). Interestingly, while RI-OH'-derived SOTs relate better to instrumental SOTs (than $TEX^L_{86}$-based SOTs), a better correlation between $TEX^L_{86}$-derived SOTs and modelled SOTs ($R^2$ = 0.64; Fig. 7e) and a weaker correlation with Ri-OH'-derived temperatures ($R^2$ = 0.55; Fig. 7f) is found.

## 5. Caveats and recommendations for future research

Marine core top studies evaluating the applicability and reliability of climate proxies are often affected by limitations and uncertainties regarding the age control of the investigated seafloor surface sediments as well as the production, preservation and degradation of target compounds. In the following, we shortly address some of these factors and provide brief recommendations for future investigations.

### 5.1 Age control

Information on the actual age of the surface sediment samples is a major requirement determining their suitability to reflect modern sea surface conditions. When comparing sea-ice conditions or ocean temperatures estimated from biomarker data obtained from 0.5-1 cm thick surface sediment samples (easily spanning decades to millennia, depending on sedimentation rates) with satellite-derived sea-ice data or instrumental records (covering only the past ~40 and 65 years, respectively), the different time periods reflected in the data sets need to be considered when interpreting the results. To address the issue of lacking age constraints for most of the surface sediments investigated here, we also performed paleoclimate simulations providing sea-ice concentration data for three time slices (2 ka, 4 ka and 6 ka BP; see Fig. S5) to evaluate if the surface sediments may have recorded significantly older environmental conditions. Correlations of $PIPSO_{25}$ values with these paleo sea-ice concentrations are notably weaker (Fig. S5) than the correlations with recent (1951-2014 CE) SIC model output, which points to a young to modern age of the majority of the studied sediments. This is further supported by AMS $^{14}$C-dating of calcareous microfossils and $^{210}$Pb-dating of seafloor surface sediments from the

553 Amundsen Sea shelf documenting recent ages for most sites (Hillenbrand et al., 2010, 2013, 2017;
554 Smith et al., 2011, 2014, 2017; Witus et al., 2014) as well as modern $^{210}$Pb-dates obtained for three
555 multicores collected in Bransfield Strait (PS97/56, PS97/68, PS97/72; Vorrath et al., 2020). AMS $^{14}$C
556 dates obtained for nearby seafloor surface sediments in the vicinity of the South Shetland Islands and
557 the Antarctic Sound revealed ages of 100 years and 142 years BP, respectively (Vorrath et al., 2019).
558 As both uncorrected ages lie within the range of the modern marine reservoir effect (e.g. Gordon and
559 Harkness, 1992), we consider these two dates still as recent. However, in an area that is significantly
560 affected by rapid climate warming over the past decades and a regionally variable sea-ice coverage, the
561 age uncertainties for at least$^{14}$C dated samples may easily lead to an over- or underestimation of
562 biomarker-based sea-ice cover and ocean temperatures, respectively, which needs to be taken into
563 account for comparisons with instrumental data. The utilization of (paleo) model data may alleviate the
564 lack of age control for each seafloor sediment sample to some extent.Nevertheless, we recommend that
565 for a robust calibration of *e.g.*, $PIPSO_{25}$ values against satellite-derived sea-ice concentrations only
566 surface sediment samples with a modern age confirmed by $^{210}$Pb-dating are incorporated.
567
568 5.2 Production and preservation of biomarkers
569 Biomarkers have the potential to reveal the former occurrence of their producers, which requires
570 knowledge of the source organisms. While there is general consensus on Thaumarchaeota being the
571 major source for iso-GDGTs (Fietz et al., 2020 and references therein) and diatoms synthesizing HBIs
572 (Volkman 2006), the main source of brassicasterol, which is not only found in diatoms but also in
573 dinoflagellates and haptophytes (Volkman 2006), remains unclear. Accordingly, the use of
574 brassicasterol to determine the $PIPSO_{25}$ index may introduce uncertainties regarding the environmental
575 information recorded by this phytoplankton biomarker. A further aspect concerns the different chemical
576 structures of HBIs and sterols, which raises the risk of a selective degradation (see Belt, 2018 and
577 Rontani et al., 2018; 2019 for detailed discussion) with potentially considerable effects on the $PIPSO_{25}$
578 index. Regarding the different areas investigated in our study, also spatially different microbial
579 communities and varying depositional regimes, such as sedimentation rate, redox conditions and water
580 depth, may lead to different degradation patterns. This means that variations in the biomarker

concentrations between different areas may not strictly reflect changes in the production of these compounds (driven by sea surface conditions) but may also relate to different degradation states. In particular, lower sedimentation rates and thus extended oxygen exposure times promote chemical alteration and degradation processes (Hedges et al., 1990; Schouten et al., 2013). However, it has been previously reported that the formation of mineral aggregates and fecal pellets often accelerates the transport of organic matter from the sea surface through the water column to the seafloor during the melting season, leading to a more rapid burial and hence better preservation of the organic compounds (Bauerfeind et al., 2005; Etourneau et al., 2019; Müller et al., 2011).

Another rather technical drawback concerning the use of the $PIPSO_{25}$ index occurs when the concentrations of the sea-ice proxy $IPSO_{25}$ and the phytoplankton marker are similarly low (due to unfavourable conditions for both ice algae and phytoplankton) or similarly high (due to a significant seasonal shift in sea-ice cover and/or stable ice edge conditions). This may lead to similar $PIPSO_{25}$ values, although the sea-ice conditions are fundamentally different from each other. This scenario is evident for five sampling sites in the Weddell Sea (PS111/13-2, /15-1, /16-3, /29-3, and /40-2; Fig. 3b+c), where $IPSO_{25}$ and the HBI Z-triene concentrations are close to the detection limit and $P_ZIPSO_{25}$ values are very low, suggesting a reduced sea-ice cover. Satellite and model data, however, show that these sample locations are influenced by heavy, nearly year-round sea-ice cover. We conclude that biomarker concentrations of both biomarkers at or close to the detection limit need to be treated with caution. Here, we assigned a maximum $P_ZIPSO_{25}$ value of 1 to those samples, and we note that such a practice always needs to be clarified when applying the $PIPSO_{25}$ approach. Nonetheless, the coupling of $IPSO_{25}$ with a phytoplankton marker provides more reliable sea-ice reconstructions. Regarding all these ambiguities, we recommend not only to calculate the $PIPSO_{25}$ index, but also to carefully consider individual biomarker concentrations and, if possible, to utilize other sea-iceproxies, such as data from well-preserved diatom assemblages (Lamping et al., 2020; Vorrath et al., 2019; 2020). While the $PIPSO_{25}$ index is not yet a fully quantitative proxy for paleo sea-ice concentrations, several calibration iterations have been applied to the GDGT-paleothermometers (Fietz et al., 2020). As noted above, the observation of distinctly warm-biased $TEX^L_{86}$-derived SOTs calls for further efforts of regional

608 calibration studies and/or investigations of archaean adaptation strategies at different water depths and
609 under different nutrient and temperature conditions.
610
611 ### 5.3 The role of platelet ice for the production of $IPSO_{25}$
612 The sympagic, tube-dwelling, diatom *B. adeliensis* is a common constituent of Antarctic sea ice and
613 preferably flourishes in the relatively open channels of sub-ice platelet layers in near-shore locations
614 covered by fast ice (Medlin, 1990; Riaux-Gobin and Poulin, 2004). Based on investigations of sea-ice
615 samples from the Southern Ocean, Belt et al. (2016) detected this diatom species to be a source of
616 $IPSO_{25}$, which, according to its habitat, led to the assumption of the sea-ice proxy being a potential
617 indicator for the presence of platelet ice. As stated above, *B. adeliensis* is not confined to platelet ice,
618 but is also observed in basal sea ice and described as well adapted to changes in the texture of sea ice
619 during ice melt (Riaux-Gobin et al., 2013). Platelet ice formation, however, plays an important role in
620 sea-ice generation along some coastal regions of Antarctica (Hoppmann et al., 2015; 2020; Lange et al.,
621 1989; Langhorne et al., 2015). In these regions, CDW and High Saline Shelf Water (HSSW) flow into
622 sub-ice shelf cavities of ice shelves and cause basal melting and the discharge of cold and less saline
623 water (Fig. 8; Hoppmann et al., 2020, Scambos et al., 2017). The surrounding water is cooled and
624 freshened and is then transported towards the surface. Under the large Filchner-Ronne and Ross ice
625 shelves the pressure relief can cause this water, called Ice Shelf Water (ISW), to be supercooled (Foldvik
626 and Kvinge, 1974). The temperature of the supercooled ISW is typically below the in-situ freezing
627 point, which eventually causes the formation of ice platelets that accumulate under landfast ice attached
628 to adjacent ice shelves (Fig. 8; Holland et al., 2007; Hoppmann et al., 2015; 2020).

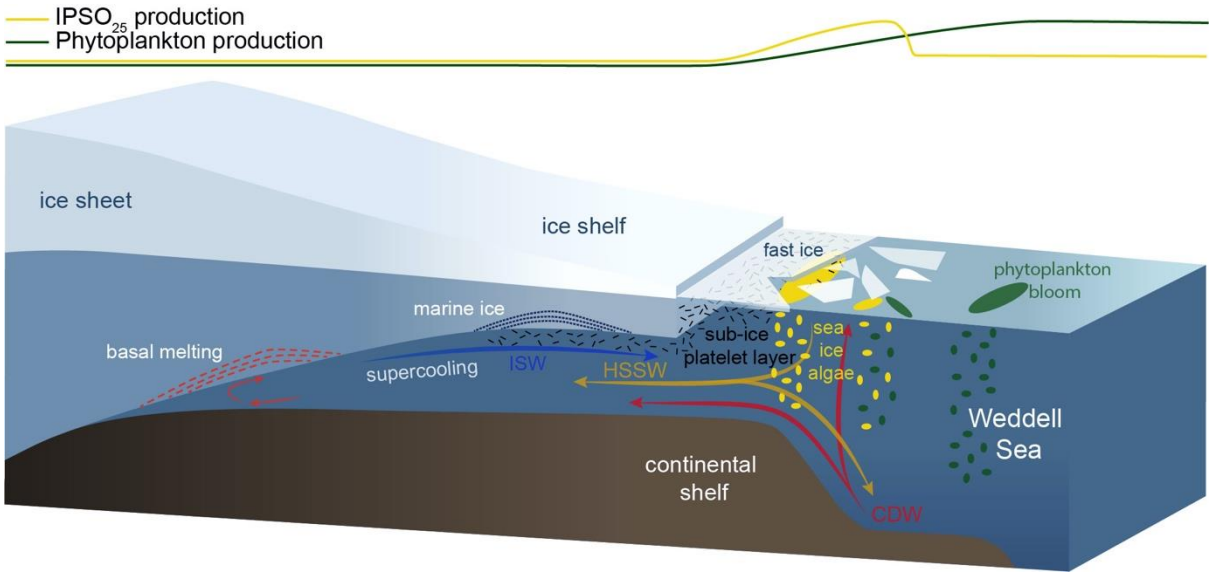


**Fig. 8:** Schematic illustration of the formation of platelet ice and the main production areas of sea ice algae producing $IPSO_{25}$ (yellow ellipses) and phytoplankton (green ellipses), also displayed by yellow and green curves at the top. CDW: Circumpolar Deep Water, HSSW: High Saline Shelf Water, ISW: Ice Shelf Water. Illustration modified from Scambos et al. (2017).

In an attempt to elucidate the relationship between $IPSO_{25}$ and platelet ice, we investigated our data in respect to locations of observed platelet iceformation. While the maximum $IPSO_{25}$ concentrations in front of the Filchner Ice Shelf could be directly related to the above-mentioned platelet ice formation in this area, the elevated $IPSO_{25}$ concentrations north of the Larsen C Ice Shelf at the EAP could be linked to several processes. According to Langhorne et al. (2015), sea-ice cores retrieved from that area did not incorporate platelet ice. The high $IPSO_{25}$ concentrations could hence be explained by either input from drift ice transported with the Weddell Gyre or by basal freeze-on. However, we note that our samples may reflect much longer time periods than the sea-ice samples investigated by Langhorne et al. (2015) and the lack of platelet ice in their investigated sea-ice cores does not rule out the former presence of platelet ice, which may be captured in our investigated sediment samples.

There are several previous studies on $IPSO_{25}$ that reported a close connection of the proxy with proximal, coastal locations and polynyas in the seasonal ice zone (*i.e.* Collins et al., 2013; Smik et al., 2016). They do not, however, discuss the relation to adjacent ice shelves as possible "platelet ice factories". We note that the core locations investigated by Smik et al. (2016) are in the vicinity of the Moscow University Ice Shelf, where Langhorne et al. (2015) did not observe platelet ice within sea-ice cores. Hoppmann et al. (2020), however, report a sea-ice core from that area, which incorporates platelet

ice. The different observations by Langhorne et al. (2015) and Hoppmann et al. (2020) highlight the temporal variability in the occurrence of platelet ice in the cold water regime around the East Antarctic margin.

For the observed $IPSO_{25}$ minimum in the Amundsen Sea (Fig. 3b; AS), which we tentatively relate to the extended and thick sea-ice coverage, the absence of platelet ice there is an alternative explanation. The Amundsen/Bellingshausen Sea and WAP shelves are classified as "warm shelves" (Thompson et al., 2018), where the upwelling of warm CDW (Schmidtko et al., 2014) hinders the formation of ISW, which makes the presence of platelet ice under recent conditions highly unlikely (Hoppmann et al., 2020). This is also supported by Langhorne et al. (2015), who stated that platelet ice formation is not observed in areas where basal ice-shelf melting is considerable, such as on the West Antarctic continental shelf in the eastern Pacific sector of the Southern Ocean (Thompson et al., 2018). Accordingly, if the formation and accumulation of platelet ice – up to a certain degree –indicates sub-ice shelf melting on "cold shelves" (Hoppmann et al., 2015; Thompson et al., 2018), high $IPSO_{25}$ concentrations found in marine sediments may hence serve as indicator of past ISW formation and associated ice shelf dynamics. Thisis, however, probably only true up to a certain threshold, where platelet ice formation decreases or is hampered due to warm oceanic conditions causing too intense sub-ice shelf melting (Langhorne et al., 2015).

When using $IPSO_{25}$ as a sea-ice proxy in Antarctica, it is important to consider regional platelet ice formation processes, too, because these may affect the $IPSO_{25}$ budget. Determining thresholds associated with platelet ice formation is challenging. Therefore, further investigations, such as in-situ measurements of $IPSO_{25}$ concentrations in platelet ice or culture experiments in laboratories, are needed to better understand the connection between $IPSO_{25}$ and platelet ice formation (and basal ice-shelf melting).

## 7. Conclusions

Biomarker analyses focusing on $IPSO_{25}$, HBI-trienes, phytosterols and GDGTs in surface sediment samples from the Antarctic continental margin were investigated to depict recent sea-ice conditions and ocean temperatures in this climate sensitive region. Proxy-based reconstructions of these key variables

were compared to (1) satellite sea-ice data, (2) instrumental ocean temperature data, and (3) modelled sea-ice patterns and ocean temperatures. The semi-quantitative sea-ice index $PIPSO_{25}$, combining the sea-ice proxy $IPSO_{25}$ with an open-water phytoplankton marker, yielded reasonably good correlations with satellite observations and numerical model results, while correlations with the sea-ice proxy $IPSO_{25}$ alone are rather low. Minimum concentrations of both biomarkers, used for the $PIPSO_{25}$ calculations, may lead to ambiguous interpretations and significant underestimations of sea-ice conditions. Therefore, different sea-ice measures should be considered when interpreting biomarker data.

Ocean temperature reconstructions based on the $TEX^{L}_{86-}$ and RI-OH'-paleothermometers show similar patterns, but different absolute temperatures. While $TEX^{L}_{86}$-derived temperatures are significantly biased towards warm temperatures in Drake Passage, the RI-OH'-derived temperature range seems more realistic when compared to temperature data based on the WOA13 and modelled annual mean SOTs.

Further investigations of HBI- as well as GDGT-synthesis, transport, deposition and preservation within the sediments would help to guide the proxies' application. Further work on the taxonomy of the $IPSO_{25}$ producers, the composition of their habitat (basal sea ice, platelet ice, brine channels) and its connection to platelet ice formation via in-situ or laboratory measurements are required to better constrain the $IPSO_{25}$ potential as a robust sea-ice biomarker. The presumed relationship between $IPSO_{25}$ and platelet ice formation in connection to sub-ice shelf melting is supported by our data, showing high $IPSO_{25}$ concentrations in areas with known platelet ice formation and low $IPSO_{25}$ concentrations in areas without observed platelet ice formation. Accordingly, oceanic conditions and the intensity of sub-ice shelf melting need to be considered when using $IPSO_{25}$ (1) as an indirect indicator for sub-ice shelf melting processes and associated ice shelf dynamics and (2) for the application of the $PIPSO_{25}$ index to estimate sea-ice coverage.

**Data availability**

Datasets related to this article can be found online on *PANGAEA Data Publisher for Earth & Environmental Science* (doi: in prep).

## Author contribution

N.L. and J.M. designed the concept of the study. N.L. carried out biomarker experiments. X.S and G.L. developed the model code and X.S. performed the simulations. C.H. provided the satellite data. M.-E.V. provided hitherto unpublished GDGT data for PS97 samples. G.M. and J.H. carried out GDGT analyses. C.-D.H. collected surface sediment samples and advised on their ages. N.L. prepared the manuscript and visualizations with contributions from all co-authors.

## Competing interests

The authors declare that they have no conflict of interest.


## Acknowledgements

Denise Diekstall, Mandy Kuck and Jonas Haase are kindly acknowledged for laboratory support. We thank the captains, crews and science parties of RV *Polarstern* cruises PS69, PS97, PS104, PS111 and PS118. Especially, Frank Niessen, Sabine Hanisch and Michael Schreck are thanked for their support during PS118. Simon Belt is acknowledged for providing the 7-HND internal standard for HBI quantification. AWI, MARUM - University of Bremen, the British Antarctic Survey and NERC UK-IODP are acknowledged for funding expedition PS104. N.L., M.-E.V. and J.M. were funded through the Helmholtz Research Grant VH-NG-1101. Two anonymous reviewers are thanked for their constructive and helpful comments, which lead to a significant improvement of this manuscript.


## References


Abernathey, R. P., Cerovecki, I., Holland, P. R., Newsom, E., Mazloff, M., and Talley, L. D.: Water-mass transformation by sea ice in the upper branch of the Southern Ocean overturning, Nature Geoscience, 9, 596-601, 2016.

Allen, C. S., Pike, J., and Pudsey, C. J.: Last glacial–interglacial sea-ice cover in the SW Atlantic and its potential role in global deglaciation, Quaternary Science Reviews, 30, 2446-2458, 2011.

727 Alonso-Sáez, L., Andersson, A., Heinrich, F., and Bertilsson, S.: High archaeal diversity in Antarctic
728 circumpolar deep waters, Environmental microbiology reports, 3, 689-697, 2011.
729 Anderson, P. S.: Evidence for an Antarctic winter coastal polynya, Antarctic science, 5, 221-226,
730 1993.
731 Armand, L. K., and Leventer, A.: Palaeo sea ice distribution–reconstruction and palaeoclimatic
732 significance, Sea ice—an introduction to its physics, biology, chemistry, and geology, 333-372,
733 2003.
734 Arrigo, K. R., Worthen, D. L., Lizotte, M. P., Dixon, P., and Dieckmann, G.: Primary production in
735 Antarctic sea ice, Science, 276, 394-397, 1997.
736 Arrigo, K. R.: Sea ice as a habitat for primary producers, Sea ice, 352-369, 2017.
737 Barbara, L., Crosta, X., Massé, G., and Ther, O.: Deglacial environments in eastern Prydz Bay, East
738 Antarctica, Quaternary Science Reviews, 29, 2731-2740, 2010.
739 Barbara, L., Crosta, X., Schmidt, S., and Massé, G.: Diatoms and biomarkers evidence for major
740 changes in sea ice conditions prior the instrumental period in Antarctic Peninsula, Quaternary
741 Science Reviews, 79, 99-110, 2013.
742 Bauerfeind, E., Leipe, T. and Ramseier, R.O.: Sedimentation at the permanently ice-covered
743 Greenland continental shelf (74°57.7'N/12°58.7'W): significance of biogenic and lithogenic
744 particles in particulate matter flux. Journal of Marine Systems 56, 151-166, 2005.
745 Belt, S. T., Allard, W. G., Massé, G., Robert, J.-M., and Rowland, S. J.: Highly branched isoprenoids
746 (HBIs): identification of the most common and abundant sedimentary isomers, Geochimica et
747 Cosmochimica Acta, 64, 3839-3851, 2000.
748 Belt, S. T., and Müller, J.: The Arctic sea ice biomarker $IP_{25}$: a review of current understanding,
749 recommendations for future research and applications in palaeo sea ice reconstructions,
750 Quaternary Science Reviews, 79, 9-25, 2013.
751 Belt, S. T., Brown, T. A., Ampel, L., Cabedo-Sanz, P., Fahl, K., Kocis, J. J., Masse, G., Navarro-
752 Rodriguez, A., Ruan, J., and Xu, Y.: An inter-laboratory investigation of the Arctic sea ice
753 biomarker proxy $IP_{25}$ in marine sediments: key outcomes and recommendations, Climate of the
754 Past., 10, 155-166, 2014.

Belt, S. T., Cabedo-Sanz, P., Smik, L., Navarro-Rodriguez, A., Berben, S. M. P., Knies, J., and Husum, K.: Identification of paleo Arctic winter sea ice limits and the marginal ice zone: Optimised biomarker-based reconstructions of late Quaternary Arctic sea ice, Earth and Planetary Science Letters, 431, 127-139, 2015.

Belt, S. T., Smik, L., Brown, T. A., Kim, J. H., Rowland, S. J., Allen, C. S., Gal, J. K., Shin, K. H., Lee, J. I., and Taylor, K. W. R.: Source identification and distribution reveals the potential of the geochemical Antarctic sea ice proxy $IPSO_{25}$, Nature Communications, 7, 12655, https://doi.org/10.1038/ncomms12655, 2016.

Belt, S. T., Brown, T. A., Smik, L., Tatarek, A., Wiktor, J., Stowasser, G., Assmy, P., Allen, C. S., and Husum, K.: Identification of $C_{25}$ highly branched isoprenoid (HBI) alkenes in diatoms of the genus Rhizosolenia in polar and sub-polar marine phytoplankton, Organic Geochemistry, 110, 65-72, 2017.

Belt, S. T.: Source-specific biomarkers as proxies for Arctic and Antarctic sea ice, Organic Geochemistry, 125, 277-298, 2018.

Berger, A.: Long-term variations of daily insolation and Quaternary climatic changes, Journal of the atmospheric sciences, 35, 2362-2367, 1978.

Blain, S., Quéguiner, B., Armand, L., Belviso, S., Bombled, B., Bopp, L., Bowie, A., Brunet, C., Brussaard, C., Carlotti, F., Christaki, U., Corbière, A., Durand, I., Ebersbach, F., Fuda, J.-L., Garcia, N., Gerringa, L., Griffiths, B., Guigue, C., Guillerm, C., Jacquet, S., Jeandel, C., Laan, P., Lefèvre, D., Lo Monaco, C., Malits, A., Mosseri, J., Obernosterer, I., Park, Y.-H., Picheral, M., Pondaven, P., Remenyi, T., Sandroni, V., Sarthou, G., Savoye, N., Scouarnec, L., Souhaut, M., Thuiller, D., Timmermans, K., Trull, T., Uitz, J., van Beek, P., Veldhuis, M., Vincent, D., Viollier, E., Vong, L. and Wagener, T.: Effect of natural iron fertilization on carbon sequestration in the Southern Ocean. Nature 446, 1070-1074, 2007.

Boon, J. J., Rijpstra, W. I. C., de Lange, F., De Leeuw, J., Yoshioka, M., and Shimizu, Y.: Black Sea sterol—a molecular fossil for dinoflagellate blooms, Nature, 277, 125-127, 1979.

781 Cavalieri, D., Parkinson, C., Gloersen, P., and Zwally, H.: Sea ice concentrations from Nimbus-7
782 SMMR and DMSP SSM/I passive microwave data, National Snow and Ice Data Center, Boulder,
783 Colorado, USA, 1996.
784 Collares, L. L., Mata, M. M., Kerr, R., Arigony-Neto, J., and Barbat, M. M.: Iceberg drift and ocean
785 circulation in the northwestern Weddell Sea, Antarctica, Deep Sea Research Part II: Topical
786 Studies in Oceanography, 149, 10-24, 2018.
787 Colleoni, F., De Santis, L., Siddoway, C. S., Bergamasco, A., Golledge, N. R., Lohmann, G.,
788 Passchier, S., and Siegert, M. J.: Spatio-temporal variability of processes across Antarctic ice-
789 bed–ocean interfaces, Nature Communications, 9, 2289, https://doi.org/10.1038/s41467-018-
790 04583-0, 2018.
791 Collins, L. G., Allen, C. S., Pike, J., Hodgson, D. A., Weckström, K., and Massé, G.: Evaluating
792 highly branched isoprenoid (HBI) biomarkers as a novel Antarctic sea-ice proxy in deep ocean
793 glacial age sediments, Quaternary Science Reviews, 79, 87-98, 2013.
794 Comiso, J. C., Gersten, R. A., Stock, L. V., Turner, J., Perez, G. J., and Cho, K.: Positive Trend in
795 the Antarctic Sea Ice Cover and Associated Changes in Surface Temperature, Journal of Climate,
796 30, 2251-2267, 2017.
797 Cook, A.J., Holland, P., Meredith, M., Murray, T., Luckman, A., Vaughan, D.G.: Ocean forcing of
798 glacier retreat in the WAP. Science, 353, 283-286, 2016.
799 Crosta, X., Pichon, J. J., and Burckle, L.: Application of modern analog technique to marine
800 Antarctic diatoms: Reconstruction of maximum sea-ice extent at the Last Glacial Maximum,
801 Paleoceanography and Paleoclimatology, 13, 284-297, 1998.
802 Crosta, X., Etourneau, J., Orme, L.C., Dalaiden, Q., Campagne, P., Swingedouw, D., Goosse, H.,
803 Massé, G., Miettinen, A., McKay, R.M., Dunbar, R.B., Escutia, C. and Ikehara, M.: Multi-
804 decadal trends in Antarctic sea-ice extent driven by ENSO–SAM over the last 2,000 years. Nature
805 Geoscience 14, 156-160, 2021.
806 Danilov, S., Sidorenko, D., Wang, Q., and Jung, T.: The Finite-volumE Sea ice–Ocean Model
807 (FESOM2), Geosci. Model Dev., 10, 765-789, 2017.de Jong, J., Schoemann, V., Lannuzel, D.,
808 Croot, P., de Baar, H. and Tison, J.-L.: Natural iron fertilization of the Atlantic sector of the

809 Southern Ocean by continental shelf sources of the Antarctic Peninsula. Journal of Geophysical
810 Research: Biogeosciences 117, 2012.
811 Denis, D., Crosta, X., Barbara, L., Massé, G., Renssen, H., Ther, O., and Giraudeau, J.: Sea ice and
812 wind variability during the Holocene in East Antarctica: insight on middle–high latitude coupling,
813 Quaternary Science Reviews, 29, 3709-3719, 2010.
814 Dorschel, B.: The Expedition PS118 of the Research Vessel POLARSTERN to the Weddell Sea in
815 2019, Berichte zur Polar-und Meeresforschung = Reports on polar and marine research, 735,
816 2019.
817 Doty, M. S., and Oguri, M.: The island mass effect, ICES Journal of Marine Science, 22, 33-37,
818 1956.
819 Eayrs, C., Li, X., Raphael, M.N. and Holland, D.M.: Rapid decline in Antarctic sea ice in recent
820 years hints at future change. Nature Geoscience 14, 460-464, 2021.
821 Esper, O., and Gersonde, R.: New tools for the reconstruction of Pleistocene Antarctic sea ice,
822 Palaeogeography, Palaeoclimatology, Palaeoecology, 399, 260-283, 2014.
823 Etourneau, J., Collins, L. G., Willmott, V., Kim, J.-H., Barbara, L., Leventer, A., Schouten, S.,
824 Damsté, J. S., Bianchini, A., and Klein, V.: Holocene climate variations in the WAP: evidence
825 for sea ice extent predominantly controlled by changes in insolation and ENSO variability,
826 Climate of the Past, 9, 1431-1446, 2013.
827 Etourneau, J., Sgubin, G., Crosta, X., Swingedouw, D., Willmott, V., Barbara, L., Houssais, M.-N.,
828 Schouten, S., Damsté, J.S.S., Goosse, H.: Ocean temperature impact on ice shelf extent in the
829 eastern Antarctic Peninsula. Nature Communications 10, 1-8, 2019.
830 Fahl, K., and Stein, R.: Modern seasonal variability and deglacial/Holocene change of central Arctic
831 Ocean sea-ice cover: new insights from biomarker proxy records, Earth and Planetary Science
832 Letters, 351, 123-133, 2012.
833 Fetterer, F., Knowles, K., Meier, W., Savoie, M., Windnagel, A.K., 2016. Updated Daily. Sea Ice
834 Index, Version 2. [Median Sea Ice Extent 1981-2010]. NSIDC: National Snow and Ice Data
835 Center, Boulder, Colorado USA. https://doi.org/10.7265/N5736NV7 [24 July 2017].

Fietz, S., Huguet, C., Rueda, G., Hambach, B., and Rosell-Melé, A.: Hydroxylated isoprenoidal GDGTs in the Nordic Seas, Marine Chemistry, 152, 1-10, 2013.

Fietz, S., Ho, S., and Huguet, C.: Archaeal Membrane Lipid-Based Paleothermometry for Applications in Polar Oceans, Oceanography, 33, 104-114, 2020.

Foldvik, A., and Kvinge, T.: Conditional instability of sea water at the freezing point, Deep Sea Research and Oceanographic Abstracts, 21, 169-174, 1974.

Fretwell, P., Pritchard, H.D., Vaughan, D.G., 57 others. Bedmap2: improved ice bed, surface and thickness datasets for Antarctica. Cryosphere 7, 375-393. http://dx.doi.org/10.5194/tc-7-375-2013, 2013.

Gersonde, R., and Zielinski, U.: The reconstruction of late Quaternary Antarctic sea-ice distribution—the use of diatoms as a proxy for sea-ice, Palaeogeography, Palaeoclimatology, Palaeoecology, 162, 263-286, 2000.

Gohl, K.: The expedition ANTARKTIS-XXIII/4 of the research vessel Polarstern in 2006, Berichte zur Polar-und Meeresforschung (Reports on Polar and Marine Research), 557, 2007.

Gohl, K.: The Expedition PS104 of the Research Vessel POLARSTERN to the Amundsen Sea in 2017, Berichte zur Polar-und Meeresforschung = Reports on polar and marine research, 712, 2017.

Gordon, J.E., Harkness, D.D.: Magnitude and geographic variation of the radiocarbon content in Antarctic marine life: implications for reservoir corrections in radiocarbon dating, Quaternary Science Reviews 11, 697-708, 1992.

Hancke, K., Lund-Hansen, L. C., Lamare, M. L., Højlund Pedersen, S., King, M. D., Andersen, P., and Sorrell, B. K.: Extreme low light requirement for algae growth underneath sea ice: A case study from Station Nord, NE Greenland, Journal of Geophysical Research: Oceans, 123, 985-1000, 2018.

Harms, S., Fahrbach, E., and Strass, V. H.: Sea ice transports in the Weddell Sea, Journal of Geophysical Research: Oceans, 106, 9057-9073, 2001.

Hedges, J.I., Hu, F.S., Devol, A.H., Hartnett, H.E., Tsamakis, E. and Keil, R.G.: Sedimentary organic matter preservation; a test for selective degradation under oxic conditions. Am J Sci 299, 529-555, 1999.

Hellmer, H.H., Rhein, M., Heinemann, G., Abalichin, J., Abouchami, W., Baars, O., Cubasch, U., Dethloff, K., Ebner, L., Fahrbach, E., Frank, M., Gollan, G., Greatbatch, R.J., Grieger, J., Gryanik, V.M., Gryschka, M., Hauck, J., Hoppema, M., Huhn, O., Kanzow, T., Koch, B.P., König-Langlo, G., Langematz, U., Leckebusch, G.C., Lüpkes, C., Paul, S., Rinke, A., Rost, B., van der Loeff, M.R., Schröder, M., Seckmeyer, G., Stichel, T., Strass, V., Timmermann, R., Trimborn, S., Ulbrich, U., Venchiarutti, C., Wacker, U., Willmes, S. and Wolf-Gladrow, D.: Meteorology and oceanography of the Atlantic sector of the Southern Ocean - a review of German achievements from the last decade. Ocean Dynamics 66, 1379-1413, 2016.

Hillenbrand, C.-D., Smith, J.A., Kuhn, G., Esper, O., Gersonde, R., Larter, R.D., Maher, B., Moreton, S.G., Shimmield, T.M., Korte, M.: Age assignment of a diatomaceous ooze deposited in the western Amundsen Sea Embayment after the Last Glacial Maximum. Journal of Quaternary Science 25, 280-295, 2010.

Hillenbrand, C.-D., Kuhn, G., Smith, J.A., Gohl, K., Graham, A.G.C., Larter, R.D., Klages, J.P., Downey, R., Moreton, S.G., Forwick, M., Vaughan, D.G.: Grounding-line retreat of the West Antarctic Ice Sheet from inner Pine Island Bay. Geology 41, 35-38, 2013.

Hillenbrand, C.-D., Smith, J.A., Hodell, D.A., Greaves, M., Poole, C.R., Kender, S., Williams, M., Andersen, T.J., Jernas, P.E., Elderfield, H., Klages, J.P., Roberts, S.J., Gohl, K., Larter, R.D., Kuhn, G.: West Antarctic Ice Sheet retreat driven by Holocene warm water intrusions. Nature 547, 43–48, 2017.

Ho, S. L., Mollenhauer, G., Fietz, S., Martínez-Garcia, A., Lamy, F., Rueda, G., Schipper, K., Méheust, M., Rosell-Melé, A., Stein, R., and Tiedemann, R.: Appraisal of $TEX_{86}$ and thermometries in subpolar and polar regions, Geochimica et Cosmochimica Acta, 131, 213-226, 2014.

Hobbs, W. R., Massom, R., Stammerjohn, S., Reid, P., Williams, G., and Meier, W.: A review of recent changes in Southern Ocean sea ice, their drivers and forcings, Global and Planetary Change, 143, 228-250, 2016.

Holland, P. R., Feltham, D. L., and Jenkins, A.: Ice shelf water plume flow beneath Filchner-Ronne Ice Shelf, Antarctica, Journal of Geophysical Research: Oceans, 112, https://doi.org/10.1029/2006JC003915, 2007.

Hopmans, E. C., Weijers, J. W., Schefuß, E., Herfort, L., Damsté, J. S. S., and Schouten, S.: A novel proxy for terrestrial organic matter in sediments based on branched and isoprenoid tetraether lipids, Earth and Planetary Science Letters, 224, 107-116, 2004.

Hoppmann, M., Nicolaus, M., Paul, S., Hunkeler, P. A., Heinemann, G., Willmes, S., Timmermann, R., Boebel, O., Schmidt, T., and Kühnel, M.: Ice platelets below Weddell Sea landfast sea ice, Annals of Glaciology, 56, 175-190, 2015.

Hoppmann, M., Richter, M. E., Smith, I. J., Jendersie, S., Langhorne, P. J., Thomas, D. N., and Dieckmann, G. S.: Platelet ice, the Southern Ocean's hidden ice: a review, Annals of Glaciology, 1-28, 2020.

Huguet, C., de Lange, G. J., Gustafsson, Ö., Middelburg, J. J., Damsté, J. S. S., and Schouten, S.: Selective preservation of soil organic matter in oxidized marine sediments (Madeira Abyssal Plain), Geochimica et Cosmochimica Acta, 72, 6061-6068, 2008.

Iacono, M. J., Delamere, J. S., Mlawer, E. J., Shephard, M. W., Clough, S. A., and Collins, W. D.: Radiative forcing by long-lived greenhouse gases: Calculations with the AER radiative transfer models, Journal of Geophysical Research: Atmospheres, 113, https://doi.org/10.1029/2008JD009944, 2008.

Jacobs, S. S., Jenkins, A., Giulivi, C. F., and Dutrieux, P.: Stronger ocean circulation and increased melting under Pine Island Glacier ice shelf, Nature Geoscience, 4, 519-523, 2011.

Jenkins, A., and Jacobs, S.: Circulation and melting beneath George VI ice shelf, Antarctica, Journal of Geophysical Research: Oceans, 113, https://doi.org/10.1029/2007JC004449, 2008.

Johns, L., Wraige, E., Belt, S., Lewis, C., Massé, G., Robert, J.-M., and Rowland, S.: Identification of a $C_{25}$ highly branched isoprenoid (HBI) diene in Antarctic sediments, Antarctic sea-ice diatoms and cultured diatoms, Organic Geochemistry, 30, 1471-1475, 1999.

Kalanetra, K. M., Bano, N., and Hollibaugh, J. T.: Ammonia-oxidizing Archaea in the Arctic Ocean and Antarctic coastal waters, Environmental Microbiology, 11, 2434-2445, 2009.

Khazendar, A., Rignot, E., Schroeder, D.M., Seroussi, H., Schodlok, M.P., Scheuchl, B., Mouginot, J., Sutterley, T.C., Velicogna, I.: Rapid submarine ice melting in the grounding zones of ice shelves in West Antarctica. Nature communications 7, 1-8, 2016.

Kim, J.-H., Van der Meer, J., Schouten, S., Helmke, P., Willmott, V., Sangiorgi, F., Koç, N., Hopmans, E. C., and Damsté, J. S. S.: New indices and calibrations derived from the distribution of crenarchaeal isoprenoid tetraether lipids: Implications for past sea surface temperature reconstructions, Geochimica et Cosmochimica Acta, 74, 4639-4654, 2010.

Kim, J.-H., Crosta, X., Willmott, V., Renssen, H., Bonnin, J., Helmke, P., Schouten, S., and Sinninghe Damsté, J. S.: Holocene subsurface temperature variability in the eastern Antarctic continental margin, Geophysical Research Letters, 39, https://doi.org/10.1029/2012GL051157, 2012.

Klinck, J. M., Hofmann, E. E., Beardsley, R. C., Salihoglu, B., and Howard, S.: Water-mass properties and circulation on the WAP Continental Shelf in Austral Fall and Winter 2001, Deep Sea Research Part II: Topical Studies in Oceanography, 51, 1925-1946, 2004.

Köhler, P., Nehrbass-Ahles, C., Schmitt, J., Stocker, T. F., and Fischer, H.: A 156 kyr smoothed history of the atmospheric greenhouse gases $CO_2$, $CH_4$, and $N_2O$ and their radiative forcing, Earth Syst. Sci. Data, 9, 363-387, 2017.

Lamping, N., Müller, J., Esper, O., Hillenbrand, C.-D., Smith, J. A., and Kuhn, G.: Highly branched isoprenoids reveal onset of deglaciation followed by dynamic sea-ice conditions in the western Amundsen Sea, Antarctica, Quaternary Science Reviews, 228, https://doi.org/10.1016/j.quascirev.2019.106103, 2020.

Lange, M., Ackley, S., Wadhams, P., Dieckmann, G., and Eicken, H.: Development of sea ice in the Weddell Sea, Annals of Glaciology, 12, 92-96, 1989.

Langhorne, P., Hughes, K., Gough, A., Smith, I., Williams, M., Robinson, N., Stevens, C., Rack, W., Price, D., and Leonard, G.: Observed platelet ice distributions in Antarctic sea ice: An index for ocean-ice shelf heat flux, Geophysical Research Letters, 42, 5442-5451, 2015.

Leventer, A.: The fate of Antarctic "sea ice diatoms" and their use as paleoenvironmental indicators, Antarctic sea ice. Biological processes, interactions and variability, 121-137, 1998.

Li, X., Holland, D.M., Gerber, E.P. and Yoo, C.:Impacts of the north and tropical Atlantic Ocean on the Antarctic Peninsula and sea ice. Nature 505, 538-542, 2014.

Liu, J., Curry, J. A., and Martinson, D. G.: Interpretation of recent Antarctic sea ice variability, Geophysical Research Letters, 31, https://doi.org/10.1029/2003GL018732, 2004.

Liu, R., Han, Z., Zhao, J., Zhang, H., Li, D., Ren, J., Pan, J., Zhang, H.: Distribution and source of glycerol dialkyl glycerol tetraethers (GDGTs) and the applicability of GDGT-based temperature proxies in surface sediments of Prydz Bay, East Antarctica. Polar Research, 2020.

Locarnini, R. A., Mishonov, A. V., Antonov, J. I., Boyer, T. P., Garcia, H. E., Baranova, O. K., Zweng, M. M., Paver, C. R., Reagan, J. R., and Johnson, D. R.: World ocean atlas 2013. Volume 1, Temperature, NOAA Atlas NESDIS 73, 40 pp., doi: 10.7289/V55X26VD, 2013.

Lohmann, G., Butzin, M., Eissner, N., Shi, X., and Stepanek, C.: Abrupt climate and weather changes across time scales, Paleoceanography and Paleoclimatology, 35, https://doi.org/10.1029/2019PA003782, 2020.

López-García, P., Rodriguez-Valera, F., Pedrós-Alió, C., and Moreira, D.: Unexpected diversity of small eukaryotes in deep-sea Antarctic plankton, Nature, 409, 603-607, 2001.

Lorenz, S. J., and Lohmann, G.: Acceleration technique for Milankovitch type forcing in a coupled atmosphere-ocean circulation model: method and application for the Holocene, Climate Dynamics, 23, 727-743, 2004.

Lott, F.: Alleviation of stationary biases in a GCM through a mountain drag parameterization scheme and a simple representation of mountain lift forces, Monthly weather review, 127, 788-801, 1999.

Loveland, T. R., Reed, B. C., Brown, J. F., Ohlen, D. O., Zhu, Z., Yang, L., and Merchant, J. W.: Development of a global land cover characteristics database and IGBP DISCover from 1 km AVHRR data, Int. J. Remote Sens., 21, 1303-1330, 2000.

970 Lü, X., Liu, X.-L., Elling, F. J., Yang, H., Xie, S., Song, J., Li, X., Yuan, H., Li, N., and Hinrichs,
971 K.-U.: Hydroxylated isoprenoid GDGTs in Chinese coastal seas and their potential as a
972 paleotemperature proxy for mid-to-low latitude marginal seas, Organic Geochemistry, 89-90, 31-
973 43, 2015.
974 Massé, G., Belt, S. T., Crosta, X., Schmidt, S., Snape, I., Thomas, D. N., and Rowland, S. J.: Highly
975 branched isoprenoids as proxies for variable sea ice conditions in the Southern Ocean, Antarctic
976 Science, 23, 487-498, 2011.
977 Massom, R. A., Scambos, T. A., Bennetts, L. G., Reid, P., Squire, V. A., and Stammerjohn, S. E.:
978 Antarctic ice shelf disintegration triggered by sea ice loss and ocean swell, Nature, 558, 383-389,
979 2018.
980 Medlin, L.: Berkeleya spp. from Antarctic waters, including Berkeleya adeliensis, sp. nov., a new
981 tube dwelling diatom from the undersurface of sea-ice, Beihefte zur Nova Hedwigia, 100, 77-89,
982 1990.
983 Meredith, M. P., Woodworth, P. L., Chereskin, T. K., Marshall, D. P., Allison, L. C., Bigg, G. R.,
984 Donohue, K., Heywood, K. J., Hughes, C. W., and Hibbert, A.: Sustained monitoring of the
985 Southern Ocean at Drake Passage: Past achievements and future priorities, Reviews of
986 Geophysics, 49, https://doi.org/10.1029/2010RG000348, 2011.
987 Meyers, P. A.: Organic geochemical proxies of paleoceanographic, paleolimnologic, and
988 paleoclimatic processes, Organic geochemistry, 27, 213-250, 1997.
989 Moore, J. K., and Abbott, M. R.: Surface chlorophyll concentrations in relation to the Antarctic Polar
990 Front: seasonal and spatial patterns from satellite observations, Journal of Marine Systems, 37,
991 69-86, 2002.
992 Müller, J., Wagner, A., Fahl, K., Stein, R., Prange, M., and Lohmann, G.: Towards quantitative sea
993 ice reconstructions in the northern North Atlantic: A combined biomarker and numerical
994 modelling approach, Earth and Planetary Science Letters, 306, 137-148, 2011.
995 Müller, J., and Stein, R.: High-resolution record of late glacial and deglacial sea ice changes in Fram
996 Strait corroborates ice–ocean interactions during abrupt climate shifts, Earth and Planetary
997 Science Letters, 403, 446-455, 2014.

998 Nakayama, Y., Schröder, M., Hellmer, H.H.: From circumpolar deep water to the glacial meltwater
999 plume on the eastern Amundsen Shelf. Deep Sea Research Part I: Oceanographic Research
1000 Papers 77, 50-62, 2013.
1001 Nakayama, Y., Menemenlis, D., Zhang, H., Schodlok, M. and Rignot, E.: Origin of Circumpolar
1002 Deep Water intruding onto the Amundsen and Bellingshausen Sea continental shelves. Nature
1003 Communications 9, 3403, 2018.
1004 Nicholls, K. W., Østerhus, S., Makinson, K., Gammelsrød, T., and Fahrbach, E.: Ice-ocean processes
1005 over the continental shelf of the southern Weddell Sea, Antarctica: A review, Reviews of
1006 Geophysics, 47, https://doi.org/10.1029/2007RG000250, 2009.
1007 Nichols, P. D., Palmisano, A. C., Volkman, J. K., Smith, G. A., and White, D. C.: Occurrence of an
1008 isoprenoid $C_{25}$ diunasaturated alkene and high neutral lipid content in Antarctic sea-ice diatom
1009 communities 1, Journal of Phycology, 24, 90-96, 1988.
1010 Nielsdóttir, M. C., Bibby, T. S., Moore, C. M., Hinz, D. J., Sanders, R., Whitehouse, M., Korb, R.,
1011 and Achterberg, E. P.: Seasonal and spatial dynamics of iron availability in the Scotia Sea, Marine
1012 Chemistry, 130, 62-72, 2012.
1013 Nolting, R., De Baar, H., Van Bennekom, A., and Masson, A.: Cadmium, copper and iron in the
1014 Scotia Sea, Weddell Sea and Weddell/Scotia confluence (Antarctica), Marine Chemistry, 35,
1015 219-243, 1991.
1016 Orsi, A. H., Whitworth III, T., and Nowlin Jr, W. D.: On the meridional extent and fronts of the
1017 Antarctic Circumpolar Current, Deep Sea Research Part I: Oceanographic Research Papers, 42,
1018 641-673, 1995.
1019 Otto-Bliesner, B., Brady, E., Zhao, A., Brierley, C., Axford, Y., Capron, E., Govin, A., Hoffman, J.,
1020 Isaacs, E., and Kageyama, M.: Large-scale features of Last Interglacial climate: Results from
1021 evaluating the lig127k simulations for CMIP6-PMIP4, Climate of the Past, 17, 63-94, 2021.
1022 Otto-Bliesner, B. L., Braconnot, P., Harrison, S. P., Lunt, D. J., Abe-Ouchi, A., Albani, S., Bartlein,
1023 P. J., Capron, E., Carlson, A. E., and Dutton, A.: The PMIP4 contribution to CMIP6–Part 2: Two
1024 interglacials, scientific objective and experimental design for Holocene and Last Interglacial
1025 simulations, Geoscientific Model Development, 10, 3979-4003, 2017.

Park, E., Hefter, J., Fischer, G., Iversen, M. H., Ramondenc, S., Nöthig, E.-M., and Mollenhauer, G.: Seasonality of archaeal lipid flux and GDGT-based thermometry in sinking particles of high-latitude oceans: Fram Strait (79° N) and Antarctic Polar Front (50° S), Biogeosciences, 16, 2247-2268, 2019.

Parkinson, C. L., and Cavalieri, D. J.: Antarctic sea ice variability and trends, 1979-2010, The Cryosphere, 6, 871-880, 2012.

Parkinson, C. L.: A 40-y record reveals gradual Antarctic sea ice increases followed by decreases at rates far exceeding the rates seen in the Arctic, Proceedings of the National Academy of Sciences, 116, 14414-14423, 2019.

Paul, S., Willmes, S., and Heinemann, G.: Long-term coastal-polynya dynamics in the southern Weddell Sea from MODIS thermal-infrared imagery, The Cryosphere, 9, 2027-2041, 2015.

Pritchard, H., Ligtenberg, S., Fricker, H., Vaughan, D., Van den Broeke, M., and Padman, L.: Antarctic ice-sheet loss driven by basal melting of ice shelves, Nature, 484, 502-505, 2012.

Raddatz, T., Reick, C., Knorr, W., Kattge, J., Roeckner, E., Schnur, R., Schnitzler, K.-G., Wetzel, P., and Jungclaus, J.: Will the tropical land biosphere dominate the climate–carbon cycle feedback during the twenty-first century?, Climate dynamics, 29, 565-574, 2007.

Riaux-Gobin, C., and Poulin, M.: Possible symbiosis of Berkeleya adeliensis Medlin, Synedropsis fragilis (Manguin) Hasle et al. and Nitzschia lecointei Van Heurck (Bacillariophyta) associated with land-fast ice in Adélie Land, Antarctica, Diatom Research, 19, 265-274, 2004.

Riaux-Gobin, C., Dieckmann, G. S., Poulin, M., Neveux, J., Labrune, C., and Vetion, G.: Environmental conditions, particle flux and sympagic microalgal succession in spring before the sea-ice break-up in Adélie Land, East Antarctica, Polar Research, 32, https://doi.org/10.3402/polar.v32i0.19675, 2013.

Rignot, E., Mouginot, J., Scheuchl, B., Van Den Broeke, M., Van Wessem, M.J., Morlighem, M.: Four decades of Antarctic Ice Sheet mass balance from 1979–2017. Proceedings of the National Academy of Sciences 116, 1095-1103, 2019.

Rintoul, S., Hughes, C., and Olbers, D.: The Antarctic circumpolar current system, International Geophysics, 77, 271-302, 2001.

Roeckner, E., Dümenil, L., Kirk, E., Lunkeit, F., Ponater, M., Rockel, B., Sausen, R., and Schlese, U.: The Hamburg version of the ECMWF model (ECHAM), Research activities in atmospheric and oceanic modelling. CAS/JSC Working Group on Numerical Experimentation, 13, 7.1-7.4, 1989.

Rontani, J.-F., Smik, L. and Belt, S.T.: Autoxidation of the sea ice biomarker proxy $IPSO_{25}$ in the near-surface oxic layers of Arctic and Antarctic sediments, Organic Geochemistry 129, 63-76, 2019.

Rontani, J.-F., Belt, S.T. and Amiraux, R.: Biotic and abiotic degradation of the sea ice diatom biomarker $IP_{25}$ and selected algal sterols in near-surface Arctic sediments, Organic Geochemistry 118, 73-88, 2018.

Sangrà, P., Gordo, C., Hernández-Arencibia, M., Marrero-Díaz, A., Rodríguez-Santana, A., Stegner, A., Martínez-Marrero, A., Pelegrí, J. L., and Pichon, T.: The Bransfield current system, Deep Sea Research Part I: Oceanographic Research Papers, 58, 390-402, 2011.

Scambos, T. A., Bell, R. E., Alley, R. B., Anandakrishnan, S., Bromwich, D., Brunt, K., Christianson, K., Creyts, T., Das, S., and DeConto, R.: How much, how fast?: A science review and outlook for research on the instability of Antarctica's Thwaites Glacier in the 21st century, Global and Planetary Change, 153, 16-34, 2017.

Schmidt, K., Brown, T. A., Belt, S. T., Ireland, L. C., Taylor, K. W., Thorpe, S. E., Ward, P., and Atkinson, A.: Do pelagic grazers benefit from sea ice? Insights from the Antarctic sea ice proxy $IPSO_{25}$, 15, 1987-2006, 2018.

Schmidtko, S., Heywood, K. J., Thompson, A. F., and Aoki, S.: Multidecadal warming of Antarctic waters, Science, 346, 1227-1231, 2014.

Schofield, O., Brown, M., Kohut, J., Nardelli, S., Saba, G., Waite, N., and Ducklow, H.: Changes in the upper ocean mixed layer and phytoplankton productivity along the West Antarctic Peninsula, Philosophical Transactions of the Royal Society A: Mathematical, Physical and Engineering Sciences, 376, https://doi.org/10.1098/rsta.2017.0173, 2018.

Schouten, S., Hopmans, E. C., Schefuß, E., and Sinninghe Damsté, J. S.: Distributional variations in marine crenarchaeotal membrane lipids: a new tool for reconstructing ancient sea water temperatures?, Earth and Planetary Science Letters, 204, 265-274, 2002.

Schouten, S., Hopmans, E. C., and Sinninghe Damsté, J. S.: The organic geochemistry of glycerol dialkyl glycerol tetraether lipids: A review, Organic Geochemistry, 54, 19-61, 2013.

Schröder, M.: The Expedition PS111 of the Research POLARSTERN to the southern Weddell Sea in 2018, Berichte zur Polar-und Meeresforschung = Reports on polar and marine research, 718, 2018.

Sidorenko, D., Goessling, H., Koldunov, N., Scholz, P., Danilov, S., Barbi, D., Cabos, W., Gurses, O., Harig, S., and Hinrichs, C.: Evaluation of FESOM2. 0 coupled to ECHAM6. 3: Preindustrial and HighResMIP simulations, Journal of Advances in Modeling Earth Systems, 11, 3794-3815, 2019.

Smik, L., Belt, S. T., Lieser, J. L., Armand, L. K., and Leventer, A.: Distributions of highly branched isoprenoid alkenes and other algal lipids in surface waters from East Antarctica: further insights for biomarker-based paleo sea-ice reconstruction, Organic Geochemistry, 95, 71-80, 2016.

Smith, J.A., Hillenbrand, C.-D., Kuhn, G., Klages, J.P., Graham, A.G.C., Larter, R.D., Ehrmann, W., Moreton, S.G., Wiers, S., Frederichs, T.: New constraints on the timing of West Antarctic Ice Sheet retreat in the eastern Amundsen Sea since the Last Glacial Maximum. Glob. Planet. Change 112, 224-237, 2014.

Smith, J.A., Hillenbrand, C.-D., Kuhn, G., Larter, R.D., Graham, A.G.C., Ehrmann, W., Moreton, S.G., Forwick, M.: Deglacial history of the West Antarctic Ice Sheet in the western Amundsen Sea Embayment, Quaternary Science Reviews 30, 488-505, 2011.

Smith, J.A., Andersen, T., Shortt, M., Gaffney, A., Truffer, M., Stanton, T.P., Bindschadler, R., Dutrieux, P., Jenkins, A., Hillenbrand, C.-D.: Sub-ice-shelf sediments record history of twentieth-century retreat of Pine Island Glacier, Nature 541, 77-80, 2017.

Spencer-Jones, C. L., McClymont, E. L., Bale, N. J., Hopmans, E. C., Schouten, S., Müller, J., Abrahamsen, E. P., Allen, C., Bickert, T., Hillenbrand, C. D., Mawbey, E., Peck, V., Svalova, A., and Smith, J. A.: Archaeal Intact Polar Lipids in Polar Waters: A Comparison Between the

Amundsen and Scotia Seas, Biogeosciences18, 3485-3504, https://doi.org/10.5194/bg-18-3485-2021, 2021.

Stevens, B., Giorgetta, M., Esch, M., Mauritsen, T., Crueger, T., Rast, S., Salzmann, M., Schmidt, H., Bader, J., and Block, K.: Atmospheric component of the MPI-M Earth system model: ECHAM6, Journal of Advances in Modeling Earth Systems, 5, 146-172, 2013.

Stocker, T. F., Qin, D., Plattner, G.-K., Tignor, M., Allen, S. K., Boschung, J., Nauels, A., Xia, Y., Bex, V., and Midgley, P. M.: The physical science basis. Contribution of working group I to the fifth assessment report of the intergovernmental panel on climate change, Computational Geometry, 18, 95-123, 2013.

Tesi, T., Belt, S., Gariboldi, K., Muschitiello, F., Smik, L., Finocchiaro, F., Giglio, F., Colizza, E., Gazzurra, G., and Giordano, P.: Resolving sea ice dynamics in the north-western Ross Sea during the last 2.6 ka: From seasonal to millennial timescales, Quaternary Science Reviews, 237, http://dx.doi.org/10.1016/j.quascirev.2020.106299, 2020.

Thomas, D. N.: Sea ice, John Wiley & Sons, 2017.

Thompson, A. F., Heywood, K. J., Thorpe, S. E., Renner, A. H., and Trasviña, A.: Surface circulation at the tip of the Antarctic Peninsula from drifters, Journal of Physical Oceanography, 39, 3-26, 2009.

Thompson, A. F., Stewart, A. L., Spence, P., and Heywood, K. J.: The Antarctic Slope Current in a changing climate, Reviews of Geophysics, 56, 741-770, 2018.

Turner, J., Orr, A., Gudmundsson, G. H., Jenkins, A., Bingham, R. G., Hillenbrand, C.-D., and Bracegirdle, T. J.: Atmosphere-ocean-ice interactions in the Amundsen Sea Embayment, West Antarctica, Reviews of Geophysics, 55, 235-276, 2017.

Turner, J., Guarino, M.V., Arnatt, J., Jena, B., Marshall, G.J., Phillips, T., Bajish, C.C., Clem, K., Wang, Z., Andersson, T., Murphy, E.J., Cavanagh, R.: Recent Decrease of Summer Sea Ice in the Weddell Sea, Antarctica, Geophysical Research Letters 47, e2020GL087127, 2020.

Valcke, S.: The OASIS3 coupler: A European climate modelling community software, Geoscientific Model Development, 6, 373-388, 2013.

Vaughan, D. G., Marshall, G. J., Connolley, W. M., Parkinson, C., Mulvaney, R., Hodgson, D. A., King, J. C., Pudsey, C. J., and Turner, J.: Recent rapid regional climate warming on the Antarctic Peninsula, Climatic change, 60, 243-274, 2003.

Vaughan, D. G.: West Antarctic Ice Sheet collapse–the fall and rise of a paradigm, Climatic Change, 91, 65-79, 2008.

Vernet, M., Geibert, W., Hoppema, M., Brown, P. J., Haas, C., Hellmer, H., Jokat, W., Jullion, L., Mazloff, M., and Bakker, D.: The Weddell Gyre, Southern Ocean: present knowledge and future challenges, Reviews of Geophysics, 57, 623-708, 2019.

Volkman, J. K.: Lipid markers for marine organic matter, in: Marine organic matter: Biomarkers, isotopes and DNA, Springer, 27-70, 2006.

Vorrath, M.-E., Müller, J., Esper, O., Mollenhauer, G., Haas, C., Schefuß, E., and Fahl, K.: Highly branched isoprenoids for Southern Ocean sea ice reconstructions: a pilot study from the WAP, Biogeosciences, 16, 2961-2981, 2019.

Vorrath, M.-E., Müller, J., Rebolledo, L., Cárdenas, P., Shi, X., Esper, O., Opel, T., Geibert, W., Muñoz, P., and Haas, C.: Sea ice dynamics in the Bransfield Strait, Antarctic Peninsula, during the past 240 years: a multi-proxy intercomparison study, Climate of the Past, 16, 2459-2483, 2020.

Wang, Z., Turner, J., Wu, Y., Liu, C.: Rapid Decline of Total Antarctic Sea Ice Extent during 2014–16 Controlled by Wind-Driven Sea Ice Drift. Journal of Climate 32, 5381-5395, 2019.

Witus, A.E., Branecky, C.M., Anderson, J.B., Szczuciński, W., Schroeder, D.M., Blankenship, D.D., Jakobsson, M.: Meltwater intensive glacial retreat in polar environments and investigation of associated sediments: example from Pine Island Bay, West Antarctica, Quaternary Science Reviews, 85, 99–118, 2014.

Xiao, X., Fahl, K., Müller, J., and Stein, R.: Sea-ice distribution in the modern Arctic Ocean: Biomarker records from trans-Arctic Ocean surface sediments, Geochimica et Cosmochimica Acta, 155, 16-29, 2015.

Zamelczyk, K., Rasmussen, T. L., Husum, K., Haflidason, H., de Vernal, A., Ravna, E. K., Hald, M., and Hillaire-Marcel, C.: Paleoceanographic changes and calcium carbonate dissolution in the central Fram Strait during the last 20 ka, Quaternary Research, 78, 405-416, 2012.

Zielinski, U., Gersonde, R., Sieger, R., and Fütterer, D.: Quaternary surface water temperature estimations: Calibration of a diatom transfer function for the Southern Ocean, Paleoceanography and Paleoclimatology, 13, 365-383, 1998.

Zwally, H. J.: Antarctic sea ice, 1973-1976: Satellite passive-microwave observations, Scientific and Technical Information Branch, National Aeronautics and Space, 1983.